DUST MAPPING OF SPIRAL GALAXY DISKS FROM THE HUBBLE STARSMOG SURVEY

by

SARAH BRADFORD

WILLIAM C. KEEL, COMMITTEE CHAIR
JEREMY BAILIN
DUNCAN FARRAH
PREETHI NAIR

A THESIS

Submitted in partial fulfillment of the requirements
for the degree of Master of Science
in the Department of Physics and Astronomy
in the Graduate School of
The University of Alabama

TUSCALOOSA, ALABAMA

2016

Copyright Sarah Bradford 2016
ALL RIGHTS RESERVED

ABSTRACT

Dust in spiral galaxy disks plays an important role in observations through its interaction with starlight. While arguments have been made in favor of completely opaque spiral disks as a result of the dust (see Valentijn, 1990), most subsequent studies agree that spiral galaxies include both optically thick and optically thin regions. Using the occulting-galaxies technique introduced by White & Keel (1992), we created transmission maps of nine partially overlapped galaxy systems taken from the STARSMOG (STarlight Absorption Reduction through a Survey of Multiple Occulting Galaxies) catalog to probe the optical depth in regions of backlit dust. The measurements of all nine targets show a wide range of opacities, and therefore none of them can be definitively classified as either "optically thick" or "optically thin".

In the analysis of the transmission maps of predominantly highly inclined systems, we noticed a distinct edge to the dust structure beyond which no dust was present in the foreground galaxy disk. This radius varied amongst systems but was distinct enough to be measured for three of the systems. The transmission maps also reveal a web-like pattern to the dust structure in some galaxy disks. Four of the targets showed dust structure which not only followed the pitch angle of the spiral arms, but also crossed at other various angles. This web-like pattern was only observed in systems where the foreground galaxy was of Hubble type SBc/Sc/Sbc.

While there appears to be no real trend in the statistics of transmission through backlit dust with respect to stellar mass of the galaxies, there does appear to be a correlation with respect to star formation rates. In this nine-system sample, the targets with the least star formation appear more opaque. By continuing this study for the rest of the STARSMOG targets, we will be able to determine how representative this sample is of the entire target set.

DEDICATION

I dedicate this thesis to one of my undergraduate physics professors, whose declaration that I was unsuitable for grad school not only helped motivate me over the speed bumps, but provided a lifelong lesson that technical expertise is no defense against being both factually and morally wrong.

ACKNOWLEDGMENTS

I'd like to take this opportunity to thank my advisor, Bill Keel, for his outstanding support in this endeavor. Without his knowledge and sense of humor this project would have been infinitely less exciting. I'm also grateful to my committee for their helpful suggestions and encouragement throughout this project. Huge thanks to my officemates Krista McCord and Lucas Johnson for their immense understanding and support throughout not only this project but the entirety of my graduate career. A special thanks to the greatest group of girlfriends I could have asked for, Danielle Nesbit and Brittany Falkenau, who were only ever a phone call away.

This project could not have been completed without the support of my parents, Carolyn and Jeffrey True, who believed in me when others did not. Finally, I'd like to thank my husband, Shawn Bradford, who allowed me to follow my dreams and was supportive and encouraging every step of the way. I quite literally couldn't have done this without you.

I acknowledge funding support from NASA STScI Program GO-13695.

CONTENTS

ABSTRACT ii

DEDICATION iii

ACKNOWLEDGMENTS iv

LIST OF TABLES vii

LIST OF FIGURES ix

1 INTRODUCTION 1

2 LITERATURE REVIEW 4

3 APPROACH 9

3.1 STARSMOG 9

3.2 Advantages & Disadvantages 10

4 OBSERVATIONS 12

5 METHODOLOGY 16

6 TARGET ANALYSIS 24

6.1 V005: UGC 9652 24

6.2 V014: SDSS 1021+17 25

6.3 V016: GAMA 2751 29

6.4 V022: GAMA 2597 31

6.5 V031: SDSS 0914+49 32

6.6 V037: SDSS 2205-00 34

6.7 V039: VV 191 35

6.8 V042: UGC 5870 36

6.9 V045: SDSS 2116+00 40

7 ANALYSIS 43

7.1 Web-like Structure 43

7.2 Edge of Dust 44

7.3 Transparency 48

7.4 Statistics 51

8 CONCLUSIONS 57

REFERENCES 59

LIST OF TABLES

4.1 Selected STARSMOG targets and their general properties 14
4.2 Selected STARSMOG targets and their general properties (continued) . . 15
7.1 Analysis Summary from Transmission Maps 44
7.2 Error Estimates of Transmission Maps 51

LIST OF FIGURES

2.1 Cartoon illustrating ideal geometry for occulting-galaxy technique 7

4.1 SNAPSHOT targets selected for analysis 13

5.1 VV 191: Ideal target for occulting-galaxy technique 17

5.2 Using ELLIPSE and BMODEL tasks to model spiral galaxy UGC 9652 . 18

5.3 Breakdown likely due to a strong bar in foreground spiral of UGC 9652 . 19

5.4 Applying a median filter to UGC 9652 images resolves the model breakdown 19

5.5 Example of ELLIPSE/BMODEL process unable to create accurate model 20

5.6 Exploiting symmetry to create transmission maps for background galaxy 21

5.7 Transmission maps of all targets 22

5.8 Example of Inclination Corrections Using UGC 9652 23

6.1 UGC 9652 SNAPshot image 24

6.2 UGC 9652 Transmission Map 26

6.3 UGC 9652 Transparency Plot 26

6.4 SDSS 1021 SNAPshot Image 27

6.5 SDSS 1021 Transmission Maps 27

6.6 SDSS 1021 Transparency Plots 28

6.7 GAMA 2571 SNAPshot Image 29

6.8 GAMA 2751 Transmission Map 30

6.9 GAMA 2751 Transparency Plot 30

6.10 GAMA 2597 SNAPshot Image 31

6.11 GAMA 2597 Transmission Map 32

6.12 GAMA 2597 Transparency Plot 33

6.13 SDSS 0914 SNAPshot Image 33

6.14 SDSS 0914 Transmission Map 34

6.15 SDSS 0914 Transparency Plot 35

6.16 SDSS 2205 SNAPshot Image 36

6.17 SDSS 2205 Transmission Map 37

6.18 SDSS 2205 Transparency Plot 37
6.19 VV 191 SNAPshot Image 38
6.20 VV 191 Transmission Map 38
6.21 VV 191 Transparency Plot 39
6.22 UGC 5870 SNAPshot Image 39
6.23 UGC 5870 Transmission Map 40
6.24 UGC 5870 Transparency Plot 41
6.25 SDSS 2216 SNAPshot Image 41
6.26 SDSS 2116 Transmission Map 42
6.27 SDSS 2116 Transparency Plot 42
7.1 VV 191: Evidence of web-like dust structure within backlit region 45
7.2 SDSS 1021: Evidence of web-like dust structure within backlit region . . 45
7.3 UGC 5870: Evidence of web-like dust structure within backlit region . . 46
7.4 UGC 9652: Evidence of web-like dust structure within backlit region . . 46
7.5 VV 191: Edge of dust structure from the SNAPshot image and dust map 47
7.6 SDSS 0914: Edge of dust structure from the SNAPshot image and dust map 48
7.7 SDSS 2205: Edge of dust structure from the SNAPshot image and dust map 49
7.8 Transparency plot of All Targets 50
7.9 Radius of backlit dust as a function of covering fraction at 10% transmission 52
7.10 Radius of backlit dust as a function of covering fraction at 50% transmission 52
7.11 Radius of backlit dust as a function of covering fraction at 90% transmission 53
7.12 Average radius of backlit dust vs. transmission; Organized by Hubble type 53
7.13 Log Mass versus Covering Fraction 54
7.14 Star Formation Rate versus Covering Fraction 55
7.15 Radii of backlit dust vs. transmission percentage for high/low mass galaxies 56
7.16 Radii of backlit dust vs. transmission percentage by star formation rates 56

CHAPTER 1

INTRODUCTION

The term cosmic "dust" refers to the solid, macroscopic matter which obscures starlight (and therefore baryonic matter) from our sight (Disney, 1995). The dust grains are made up of dielectric and refractory materials and are known to play an important role in the astrophysics of the interstellar medium (ISM) and galaxies as a whole (Pogge, 2015; Draine, 2003). While the physical properties of the dust grains (including composition) remain elusive, the role the dust plays on observations of the universe is obvious due to its interaction with starlight and the detectable radiation in the infrared wavelength. In the interstellar medium, an estimated 32% of starlight emitted in a galaxy is reradiated by dust (Viaene et al., 2015)!

The results of dust studies have a variety of implications on fundamental questions in astrophysics, including how dust affects observations of supernova Ia (SN Ia) for use in distance measurements and creating accurate spectral energy distribution models of galaxies. The amount of light lost to dust which absorbs and scatters light along the line of sight is currently estimated using extinction laws which are often assumed to be constant. In reality, the extinction due to dust is not a constant parameter. As a result, SN Ia extinction may be highly simplified with respect to actual extinction amounts (Holwerda, 2014). By studying the dust and its distribution within galaxies, we can apply its correction to the mean luminosity distance of SN Ia. Spectral energy distributions (SED), which measure how a star's light is reprocessed from ultra-violet (UV) and optical wavelengths to the far infrared (FIR), also depend on the distribution of the dust within a galaxy. Current SED models wildly underestimate the typical extinction at various wavelengths (specifically, the amount of reprocessed UV radiation, especially for edge-on galaxies) and total dust masses as a result of incomplete relative distributions of stars and dust (Keel et al., 2013). The Galaxy and Mass Assembly (GAMA) survey aimed to

correct this problem by constraining the distribution of the dust in addition to studying the color-size relationship in galaxies, the inclination-SED relation, and measuring the UV-slope and Balmer decrement for its survey and spectral catalog (Holwerda, 2014). Furthermore, Disney (1995) wrote about how dust studies can help answer the following fundamental astrophysics questions:

I. Are global properties of spirals disguised because we are unable to correct for dust?

II. How is our view of background galaxies affected by the dust of foreground galaxies?

III. Do uncertainties in the role of dust translate into significant uncertainties in the baryonic mass of galaxies?

IV. Can the large far infrared outputs in disk galaxies be attributed to re-processed starlight from dust?

V. How much of the dynamical evolution of galaxies is attributed to the presence and distribution of dust?

VI. How largely does dust affect the k-corrections needed to infer luminosity and spectral evolution of galaxies?

VII. How does dust affect inclination corrections to the Tully-Fisher relation?

Studying dust extinction within galaxies has proven to be a worthwhile topic because of its impact on a wide range of astrophysical issues. Mapping and measuring the dust content in galaxies is essential to understanding how the dust affects luminosity estimates and star formation rates which have dependencies on a galaxy's internal absorption. By accounting for dust, we are more equipped to observe distant objects, such as quasars, through the disk of a foreground galaxy where high enough levels of extinction would bring about questions as to the accuracy of straight-forward estimates of stellar masses and distributions (Driver et al., 2008). Dust extinction affects the extragalactic distance scale through inclination corrections to the Tully-Fisher relation based on our line of sight and also provides insight about the relationship between stars and the interstellar

medium within galaxies. Properly accounting for the effects of dust upon light from galaxies is crucial to our understanding of overall galaxy evolution.

CHAPTER 2

LITERATURE REVIEW

Effectively measuring the dust content and typical extinction in galaxies has historically been a controversial topic because various approaches have yielded considerably different results. Curtis (1918) first documented the presence of "absorbing or occulting matter" in his photographic catalog of galaxies and since then, the topic of dust in late-type galaxies has been an on-going discussion. The terms "late-type" and "early-type" typically refer to spiral/irregular galaxies and elliptical galaxies, respectively. The traditional view, based on the work of Holmberg (1958) and de Vaucouleurs et al. (1976) was that disks are effectively transparent whereas later studies by Valentijn (1990) and Disney et al. (1989) suggested the opposite (James & Puxley, 1993). These discrepancies led to the use of several new techniques, each thought to solve the issue of measuring the optical depth in late-type galaxy disks. In addition to the classical inclination surface brightness test, several new observational techniques, including studying rotation curves and using occulting-galaxy pairs, were being used to map and measure dust content in galactic systems.

The inclination surface brightness test first used by Holmberg (1958) is one of the oldest methods used to determine the opacity of spiral galaxies. This approach tested the theory that a transparent disk would have constant luminosity regardless of inclination angle, therefore the surface brightness must increase with inclination to make up for the decreased area over which the luminosity is distributed. Holmberg's data suggested a slight inclination dependence and correspondingly modest internal extinction, but the conclusion that an opaque spiral disk would have the same surface brightness regardless of its inclination (while a transparent disk would have a higher surface brightness when viewed edge-on) proved to be a controversial assumption. Valentijn (1990) used the inclination surface brightness test on a sample of nearly 9,400 ESO-LV (Lauberts

& Valentijn, 1989) galaxies where it was concluded that spirals are largely opaque (and therefore the inclination of the galaxy had no bearing on calculating the dust content), though this result and analysis was challenged by Burstein et al. (1991). Selection effects could crop up easily in the ESO-LV sample because this galaxy catalog was selected by eye from photographic survey copies. Valentijn's result seemed unreasonable given that the ESO-LV catalog itself would not have been easily obtained if all spiral galaxies were opaque, given that we live in a spiral galaxy. The fact that we have already observed distant objects (quasars, other galaxies, etc) through foreground galactic disks also makes Valentijn's result all that more questionable. Burstein et al. (1991) concluded that spiral galaxies are, in fact, optically thick though not thoroughly opaque and that while Valentijn's results were consistent with their own, the Valentijn (1990) result was due to sample selection effects. Specifically, Huizinga (1994) attributed Valentijn's results to the presence of bulge systems in the sample, which in surface brightness tests are more inclination independent. A later study done by Burstein et al. (1995) used an expanded sample and found that perhaps spiral galaxies are not so optically thick as originally thought due to a slight inclination dependence. Clearly there is residual ambiguity with the classical inclination-surface brightness test, which is perhaps why there remains interest in its result.

As early as 1989, Disney et al. (1989) challenged Holmberg's conclusion of nearly opaque spiral disks on theoretical grounds. Their approach involved comparing radiative transfer models with observed color and surface brightness data (which did not require low internal extinction) and resulted in models of dusty disks which could reproduce Holmberg's data so long as the disk scale height was much less than that of the stars. More specifically, layered models with a physically thin but optically thick dust layer behaved like optically thin discs (Disney et al., 1989). The end result was that while they couldn't prove that disk galaxies are optically thick, the visual-light evidence for their being optically thin was weak. Furthermore, similar radiative transfer models have been used to investigate the notion that reddening of broadband color increases with more dust extinction. Using similar radiative transfer models, Witt et al. (1992) investigated

the transfer of ultraviolet, visual, and near-infrared radiation within a variety of spherical geometries in an attempt to replicate the types of dusty environments often seen in galaxies. Their results were obviously sensitive to the geometry but indicated that previous work on the effects of dust on stellar radiation was often too simplistic.

Because dust extinction affects basic observable parameters used in selection criteria for statistical analysis, it is difficult to avoid biases in target selection (Byun, 1993). For that reason, new methods were introduced which were free from the same selection biases including the use of rotation curves to investigate the dust opacity. Goad & Roberts (1981) studied the morphologies, kinematics, and line ratios of edge-on galaxies and were among the first to hypothesize that an optically thick spiral disk would produce a solid-body rotation curve regardless of the shape of the actual rotation curve (because the local line-of-sight velocity measured by the Hα line is subject to how far we can see through the disk). If the disk is optically thick the observed Hα emission would come from the ionized gas near the edge of the disk, producing an apparent solid body rotation curve (Byun, 1993). Only one of the six galaxy targets studied by Goad & Roberts (1981) produced a rotation curve which varied linearly with projected radius, indicating a high optical depth. Therefore for an edge-on spiral, the shape could be an indicator of the opacity. Using the same idea that for an edge-on spiral, the shape of the rotation curve can be used as an indicator for opacity, Bosma et al. (1992) compared Hα rotation curves of two systems with their position-velocity diagrams obtained from 21 cm line observations (which are not affected by dust absorption); the idea being that an optically thick edge-on galaxy would show an apparent solid body rotation curve in Hα because the observed Hα emission would then have to come from ionized gas at the near edge of the optical disk. By comparing the optical and HI kinematics in edge-on spiral galaxies, (specifically NGC 891 and NGC 100) they concluded that spiral galaxies are transparent in at least their outer regions, and attributed the optically thick regions of large spiral galaxies to purely the amount of material present. The idea that the rotation curve of a spiral could give an indication as to the opacity was more recently discussed by Misiriotis (2005). Uncertainties in the adopted scale-height to scale-length ratio, in

the adopted velocity dispersion, and in the assumed Hα distribution yield significantly different opacities derived from studying the rotation curves of spiral galaxies.

Other methods of directly observing the dust content in spiral galaxies began to emerge as a result of attempting to avoid the requirement that the dust distribution within the galaxy (and the internal disk structure itself) be well known. Among the most successful, White & Keel (1992) attempted to directly measure the optical depth in a spiral galaxy using partially overlapped galaxy pairs in the optical wavelength, where the foreground spiral galaxy is backlit by another (ideally elliptically- or spheroidally-symmetric) galaxy (see Figure 2.1). By using differential photometry and the unobscured part of the background galaxy, they were able to measure the amount of background light lost in crossing the foreground disk and found that higher extinction exists in the arms of a spiral than in the inter-arm regions of the disk. Occulting-galaxy pairs have since been used to study many of the other effects associated with dust in spiral galaxies, including calculating the reddening curve of dust in the system (Keel & White, 2001a) and determining the extinction in disks of foreground spiral galaxies (Keel & White, 2001b; Domingue et al., 2000).

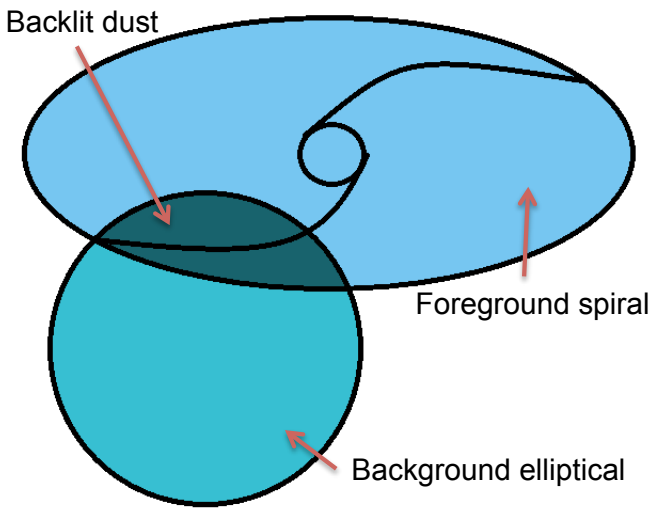

Figure 2.1: Cartoon illustrating ideal geometry for occulting-galaxy technique

Citing the disadvantages of this overlapping-galaxy method (the requirement that the background galaxy be symmetric and the fact that only a few targets exist on which this technique can be applied) González et al. (1998) introduced their own direct-observation

technique called the "Synthetic Field Method" which also did not require any *a priori* assumptions about the spatial distribution (or reddening law) of the dust. The "synthetic field" method looked for colors and counts of background galaxies through the disk of a foreground galaxy and found that in the case of NGC 4536, there was more extinction in the arms of the galaxy than in the inter-arm region, in agreement with White & Keel (1992) for a different object. These results, however, were again limited by statistics; the number of galaxies doesn't obey Poisson statistics due to the under- and over-densities in the cosmic web. It is also limited because the background galaxy numbers are not usually all that large anyway, therefore making fluctuations worse than Poisson statistics just makes a bad situation worse.

CHAPTER 3
APPROACH

3.1 STARSMOG

Thus far, the occulting-galaxy pairs method seems to be the most successful in investigating the opacity of spiral galaxies at the visual wavelength and thanks to large surveys including the Sloan Digital Sky Survey (SDSS), Galaxy Zoo, and GAMA there are many more systems on which this technique can be applied. Most recently, the STarlight Attenuation and Reddening Survey of Multiple Occulting Galaxies (STARSMOG) project has collected HST/WFC3 SNAP observations of 54 occulting-galaxy systems with various foreground galaxy mass, radius, inclination, and Hubble type, seeking to create a complete and comprehensive survey devoid of selection biases and with a wider range at higher resolution than hitherto possible from very local galaxies and a handful of targeted HST programs (Holwerda, 2014). The STARSMOG observations and resulting transmission maps are expected to have a direct impact in three fundamental areas of astrophysics. The maps are expected to:

I. Yield an extinction probability for supernova light curves in similar host galaxies. Because dust absorbs and scatters light along the line of sight, it is necessary to quantify the total amount of light lost when observing distant objects such as supernovae. The extinction laws currently being applied are often using assumed values (either flat, which has no physical grounds, or exponential) because little is known about the dependency of extinction on host galaxy type, stellar mass, galactocentric radius or inclination. By providing an extinction template for a variety of galaxies of varying physical properties, we are more equipped to estimate the mean luminosity distance of the SN Ia.

II. Strongly constrain the role of ISM structure in spectral energy distribution models of spiral galaxies. While SED models have become more accurate in recent years, current SED models still disagree with observations, especially when edge-on, and they wildly underestimate the amount of light reprocessed by dust. While the GAMA survey was tasked with attacking this problem, the relative distribution of the dust remains a free parameter. The statistical properties of the resultant transmission maps of spiral disks would represent a key constraint to this problem.

III. Map the level of ISM turbulence through the spatial power-spectrum. The physics dominating the ISM in late-type galaxies on small (turbulence due to stellar winds, supernovae feedback, and cloud self-gravity) and large scales (spiral density waves, gravitational interaction, etc.) results in a specific double-power-law power spectrum of the ISM. Prior to the STARSMOG survey, the range of scales could only be resolved for the nearest galaxies (M31, M33 and the Magellanic Clouds) observed with the European Space Agency's far-infrared space telescope, *Herschel*. This HST survey will allow us to expand this knowledge to many more galaxies to determine where turbulence and pressure are in balance with self-gravity for a range of Hubble types.

3.2 Advantages & Disadvantages

Arguably the biggest limitation to the occulting-galaxy technique is that its success depends on the symmetry of both the foreground and background galaxies. Also, while the number of potential targets has increased thanks to the SDSS, Galaxy Zoo, and GAMA surveys, there is still only a limited number of targets close enough for this type of photometric analysis. Despite these limitations, the occulting-galaxy approach to directly tracing the dust transmission comes with quite a few advantages that eliminate much of the controversial selection effects seen in statistical samples, as well as the structural assumptions required for multi-wavelength analysis. White et al. (2000) cited the following advantages to their technique:

- The approach is not conditional on the same sample selection effects that plague some statistical studies. As previously mentioned, these selection effects can vastly influence results and allow for conclusions which are purely nonsensical (see Valentijn, 1990).

- Unlike approaches using spectroscopic analysis, this technique does not require that we correct for background extinction nor does it lead to selection biases against high opacity regions. In order to extract and isolate the foreground spectra, it is necessary to correct for the extinction of the background source and for the Milky Way. Additionally, as James & Puxley (1993) discovered, spectroscopic surveys of background objects which include objects like quasars or H-II regions (or any small, point-like source) behind a spiral disk introduce a selection bias against high opacity regions.

- The technique does not require calibration corrections or therefore the need to account for their corresponding errors. This is a byproduct of doing purely differential photometry.

- This approach is not affected by color gradients. These gradients are a result of stellar population gradients and can be problematic when using color maps as dust detectors (see Block et al., 1994; González et al., 1998).

- This approach doesn't require any assumptions about the vertical structure of the disk. Elmegreen (1980) used the galaxy's own light to probe extinction but was forced to make assumptions about the distribution of stars and dust in the z-direction.

CHAPTER 4

OBSERVATIONS

The STARSMOG project used Hubble Space Telescope (HST) SNAP observations to create a catalog of occulting-galaxy pairs for foreground galaxies with various Hubble types, masses, radii and inclination. We provided a wide selection of target samples to the HST SNAP program but maintained that while more observed targets allow for better analysis, one target was not favored over another. Target selection for the STARSMOG catalog was enabled by SDSS, Galaxy Zoo and the GAMA survey, all of which alleviated the difficulty of identifying bona-fide occulting-galaxies rather than tidally-interacting systems. To further ensure the completeness for STARSMOG, strict selection criteria were established based on separation on the sky and redshift. To be considered for observation, the SNAP targets must have had:

a. A reliable GAMA or SDSS redshift for foreground and background objects

b. Reliable GAMA photometry and structural measurements of the foreground galaxy

c. A redshift difference of delta v $>$ 500 km/s to exclude interacting galaxies which may present asymmetrical error bars and contribute to the scattered light of dust.

d. A project on-sky difference of delta r $<$ 20 kpc

With these requirements, 54 targets were selected for observation with HST.

The SNAP observations for STARSMOG (HST program 13695) were single orbit, WFC3/UVIS (wide Johnson V) observations of each galaxy pair using the F606W filter. The SNAPshots were at least 700 second exposures which results in a signal-to-noise

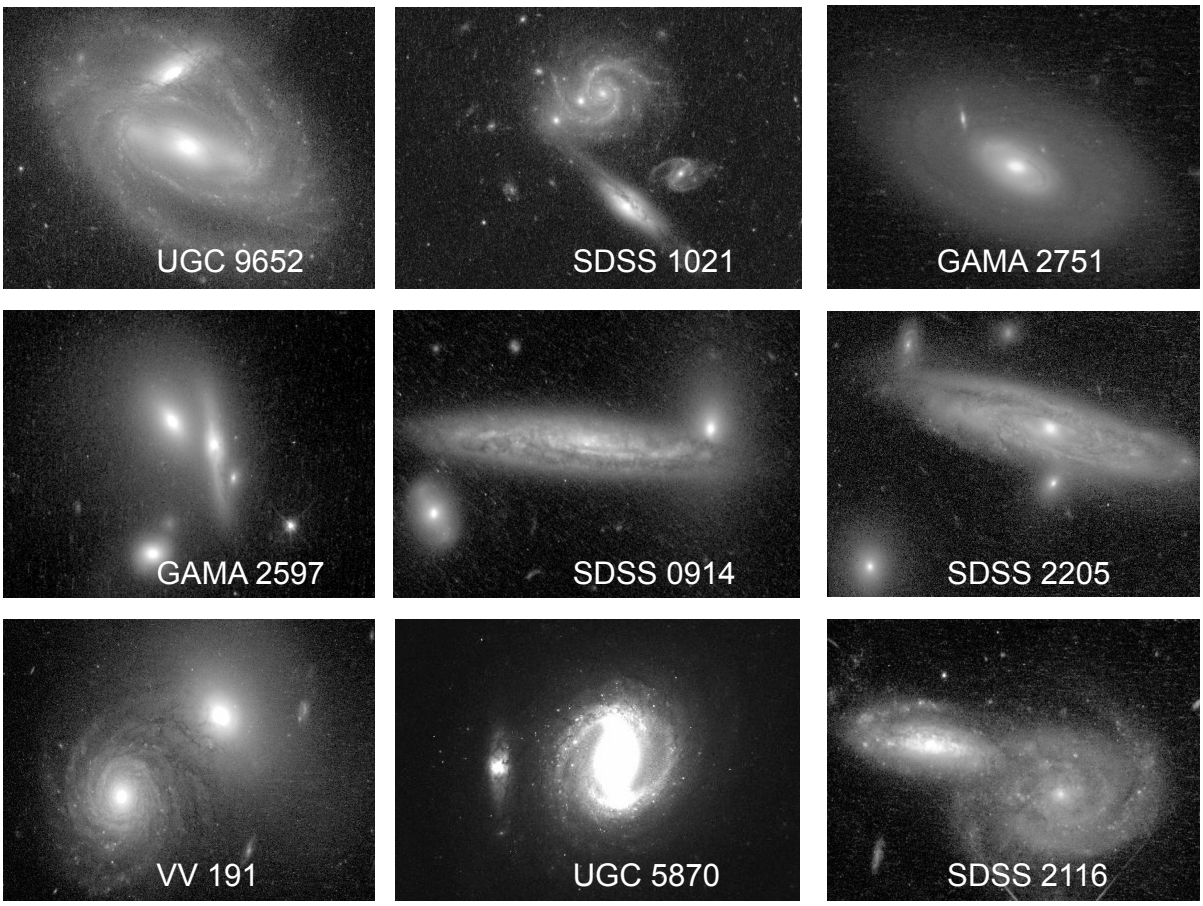

Figure 4.1: SNAPSHOT targets selected for analysis

(S/N) > 7 at the R_{25} radius of both foreground and background galaxies. It is important to note that no single target pair played a crucial role in the STARSMOG study because the end result was to create a catalog of dust distributions as a function of various physical properties of the foreground galaxy

For this study we chose 9 of the 54 STARSMOG targets which we believed would be best served using the occulting-galaxy technique to analyze the backlit dust region. Chosen because their levels of symmetry were high enough for immediate analysis with the most straight forward toos, the list of nine selected targets and their general properties can be seen in tables 4.1 and 4.2 and the SNAPshot images can be seen in figure 4.1.

Table 4.1: Selected STARSMOG targets and their general properties

Object	SDSS Object ID	Hubble Tyle (fg)	Redshift (fg)	Redshift (bg)	Inclination	Ellipticity	Axial Ratio	Petrosian Radius (arcsec)
UGC 9652	1237668298757701744	SB(r)c	0.038	0.074	63	0.55	0.45	22.22
SDSS 1021	1237668289620672636	Sc	0.0393	0.2478	37	0.203	0.797	10.05
GAMA 2751	1237651753452765233	Sab	0.0521	0.291	56	0.45	0.55	7.66
GAMA 2597	NO DATA	Dwarf-ish disk?	[a]	0.0999	65	0.57	0.43	12.13
SDSS 0914	1237654652569321688	Scd	0.0345	0.1194	45	0.293	0.707	16.25
SDSS 2205	1237663542609707303	SB(?)bc	0.0311	0.1445	43	0.27	0.73	20.07
VV 191	1237665531709096084	Sc	0.0514	0.0513	20	0.06	0.94	13.59
UGC 5870	1237664818742951977	SB(r)bc	0.0068	0.0444	31	0.14	0.86	13.4
SDSS 2116	1237663457777352875	SB(r)c	0.0318	0.0439	48	0.33	0.67	13.82

[a]The galaxy with backlit dust is not the original galaxy (with known redshift) that caused the system to be selected for this analysis.

Table 4.2: Selected STARSMOG targets and their general properties (continued)

Object	SDSS Object ID	Scale Length (arcsec)	Log Mass (Solar Masses)	Age (Gyr)	Luminosity (erg/s)	SFR (Solar Masses/yr)
UGC 9652	1237668298757701744	10.43	11.08	8.25	2.78E+39	0.0186
SDSS 1021	1237668289620672636	4.45	NO DATA	NO DATA	NO DATA	NO DATA
GAMA 2751	1237651753452765233	3.63	10.58	3.5	2.41E+39	0.0161
GAMA 2597		0.89	NO DATA	NO DATA	NO DATA	NO DATA
SDSS 0914	1237654652569321688	7.48	9.78	1.609	9.91E+39	0.066
SDSS 2205	1237663542609707303	3.88	10.25	1.434	1.67E+39	0.0111
VV 191	1237665531709096084	3.45	10.32	1.1391	6.60E+39	0.0440
UGC 5870	1237664818742951977	6.95	9.01	0.7187	NO DATA	NO DATA
SDSS 2116	1237663457777352875	2.66	10.36	13	1.15E+39	0.0077

CHAPTER 5

METHODOLOGY

The ideal target for use in directly mapping dust structure in spiral disks using the occulting-galaxies technique requires a foreground spiral which at least partially overlaps a similarly-sized background elliptical. An example of such, which happens to be a STARSMOG target used for this study can be seen in figure 5.1. By using symmetry from the non-overlapped portion of the background galaxy, we can then estimate the light from each galaxy separately and therefore reconstruct the absorption in the overlapped region of the foreground. The methods used to isolate the dust and create the resultant transmission maps are discussed here.

In order to best isolate the area where the dust of the foreground was most backlit, we used the data analysis software STSDAS offered by the Space Telescope Science Institute (STScI) for the Image Reduction and Analysis Facility (Tody, 1986, 1993) software, specifically taking advantage of the ISOPHOTE bundle which included the ELLIPSE and BMODEL tasks (STSDAS is a product of the Space Telescope Science Institute, which is operated by AURA for NASA). The ELLIPSE task uses an iterative method where each isophote is fitted using a pre-defined, fixed semi-major axis length starting from estimates of the galaxy's center coordinates, ellipticity, and position angle. The task samples the image to produce a 1-dimensional intensity distribution and analyzes the deviation of certain elliptical parameters from the "true" value at which point the parameter is updated and the image is resampled. The task continues until either the number of user-specified iterations is complete or the light from the galaxy is such that it cannot be distinguished from the background. The BMODEL task uses the isophotal analysis of the ELLIPSE task to create a 2-dimensional image file containing a photometric model of the source image (Jedrzejewski, 1987).

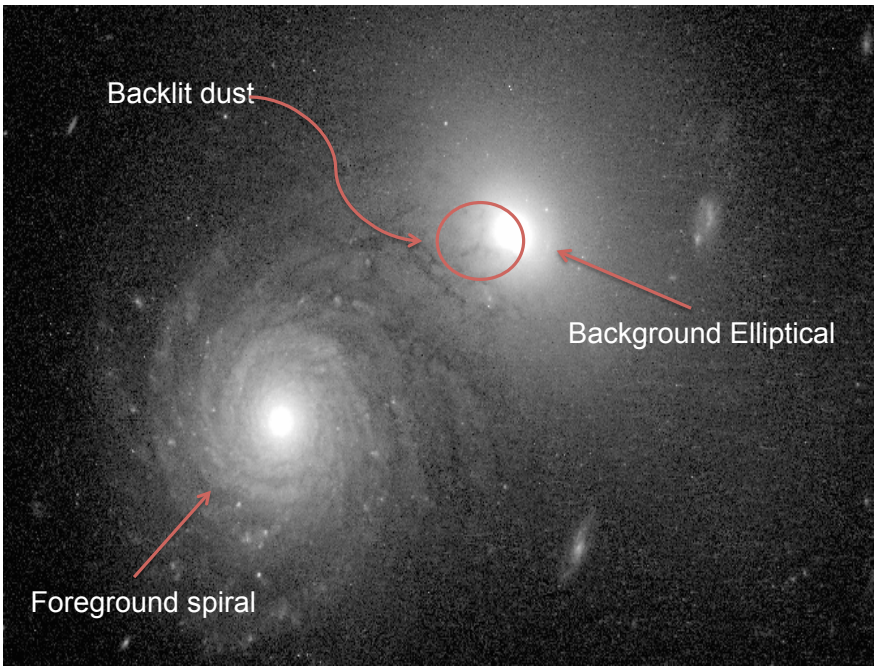

Figure 5.1: VV 191: Ideal target for occulting-galaxy technique

After sky-subtracting the SNAPshot images provided by HST, we (1) completed an ellipse-fit isophote analysis of the background using the ELLIPSE task, taking care to mask the backlit dust, the foreground galaxy, and any other objects in the image which might have tainted the ellipse fitting (i.e., stars, other unrelated galaxies, etc.). We then (2) built a model image from the results of the isophotal analysis using the BMODEL task. A sample of the BMODEL task is shown in figure 5.2. Then, by (3) subtracting the model from the initial (sky-subtracted) image, we were able to effectively "remove" the background's emission from the image leaving only residuals which were dependent on the success of the ellipse-fitting. This 3-step process was repeated (4, 5, 6) for the foreground galaxy where the resultant image left the dust untouched and where only the residuals of the foreground and background remained. Finally, to further isolate the dust we (7) divided out the model image of the foreground produced by the BMODEL task.

While the ELLIPSE and BMODEL tasks created adequate isophote models in many cases by themselves, we found that prominent dust lanes, for example, affected the gradient of the models. In such cases, we used a median filter to effectively smooth the model without changing the statistics developed by the ELLIPSE task. The filter works by using a user-defined rectangular window to "slide" across the image, replacing the center

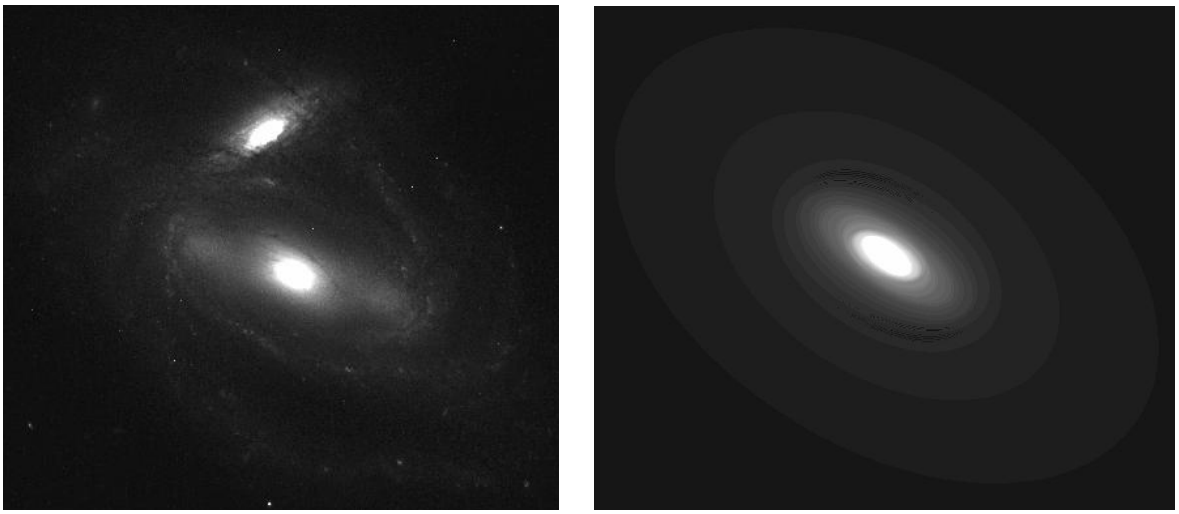

(a) Original SNAPshot Image (b) Isophote Model of Foreground Spiral

Figure 5.2: Using ELLIPSE and BMODEL tasks to model spiral galaxy UGC 9652

pixel in the window with the median value of all pixels contained within the window. The breakdown of the BMODEL task is shown in figure 5.3 for UGC 9652 where the blue boxes indicate the region where the breakdown occured and the side panels on the left show a close-up view of the same region. The end result, after having applied a median filter, can be seen in figure 5.4.

The results of isolating the dust using elliptical isophote fits are completely dependent on the ability to model each galaxy as an ellipse. In several instances the inclination or presence of a bar, for example, did not allow for such modeling. Figure 5.5 shows an example of the background galaxy in UGC 9652 where the ELLIPSE and BMODEL tasks were unable to create an accurate model. In such cases we used the symmetry of the foreground to remove its emission from the image. For a face-on spiral, rotational symmetry could be used to swing the unprojected portion around for subtraction. To do this, we utilized IRAF's ROTATE command to rotate the spiral 180 degrees about its estimated center coordinates and subtracted the rotated image from the unrotated one. This technique also worked in cases where a strong bar dominated the foreground galaxy. In the case of a particularly edge-on spiral, reflection symmetry was used to flip the unprojected portion of the spiral over for subtraction. In this case, the spiral had to first be rotated so that the spiral was parallel to either the X or Y axis and then the image was

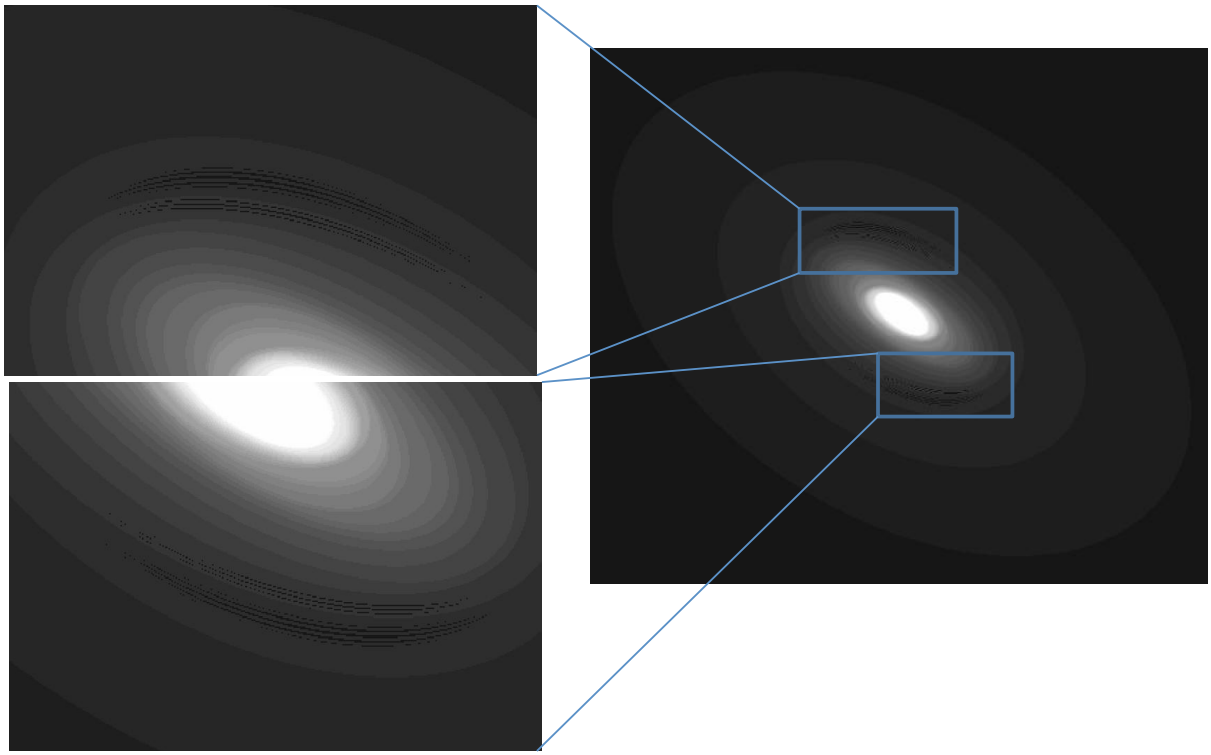

Figure 5.3: Breakdown likely due to a strong bar in foreground spiral of UGC 9652

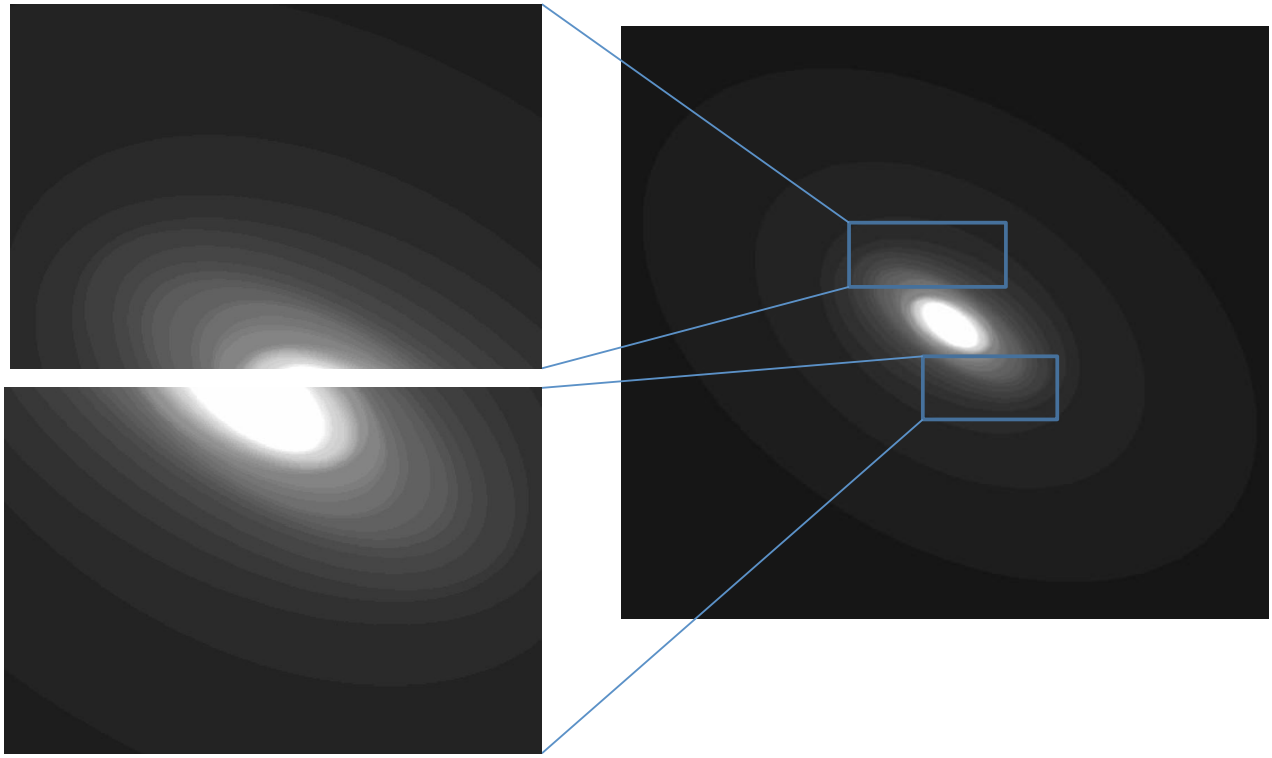

Figure 5.4: Applying a median filter to UGC 9652 images resolves the model breakdown

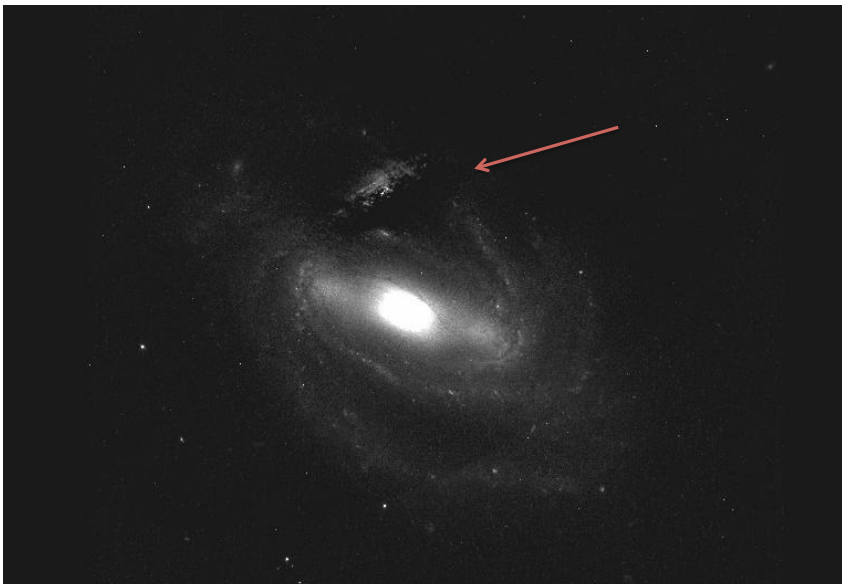

Figure 5.5: Example of ELLIPSE/BMODEL process unable to create accurate model

copied so that the resultant image was a mirrored image of the first, either symmetrical about X or Y. At this point, often times the mirrored image had to be shifted so that the foreground galaxy's center coordinates matched those of the original image. We then used image arithmetic to take the maximum of the original and mirrored images before rotating the spiral back into its original frame and dividing out the emission from the foreground. Often enough simply using 2-fold symmetry, as described above, yielded the desired result, but in some cases 4-fold symmetry (mirror about X, about Y, and about both axes) was required. An example of the images produced throughout this process is shown in figure 5.6.

Here we present dust transmission maps using the occulting-galaxy technique for nine of the best overlapping galaxy pairs from 54 targets of the STARSMOG survey. Once a reasonable transmission map was produced for each target, we investigated the properties of the dust, including the radii of the foreground galaxy at which the dust was located and its covering fraction. The final transmission maps for all nine targets are presented in figure 5.7.

The ELLIPSE task from the STScI program database generates a table which includes general information about the galaxy, including the intensity, ellipticity and semi-major axis of each elliptical isophote. For very near-edge-on galaxies or other cases where the

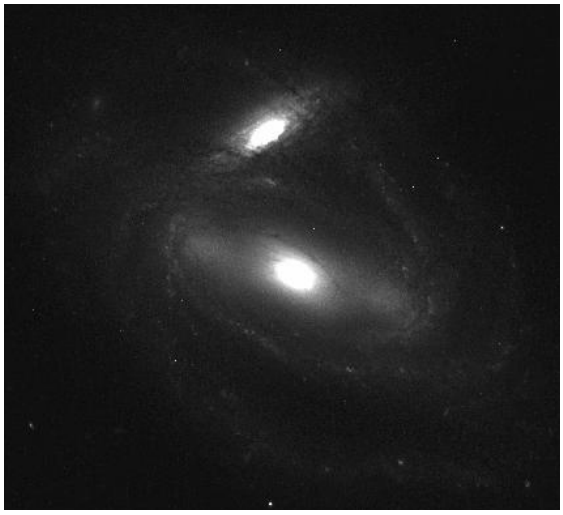

(a) Original SNAPHOT image

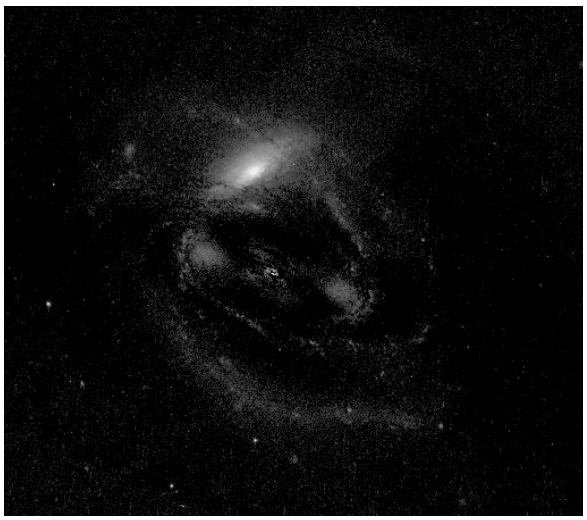

(b) Emission from foreground removed

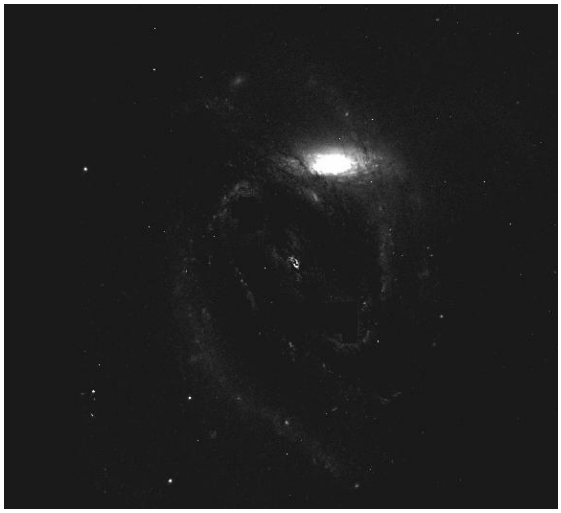

(c) Step 1: Align galaxy with rotation axis

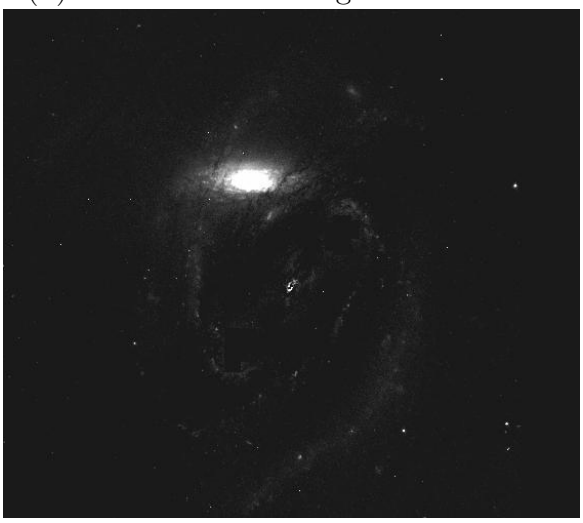

(d) Step 2: Mirror image across rotation axis

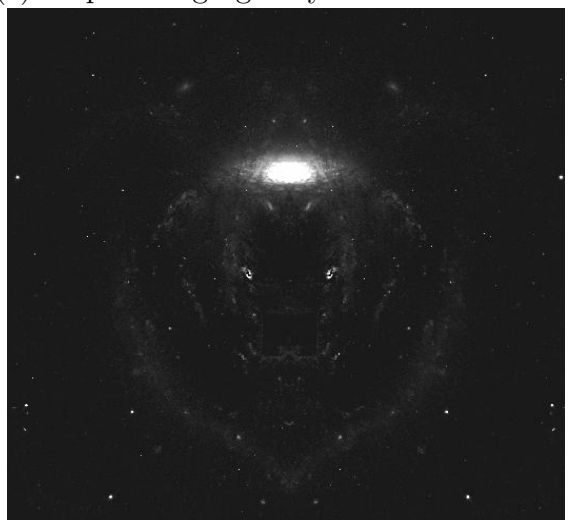

(e) Step 3: Display maximum pixel value

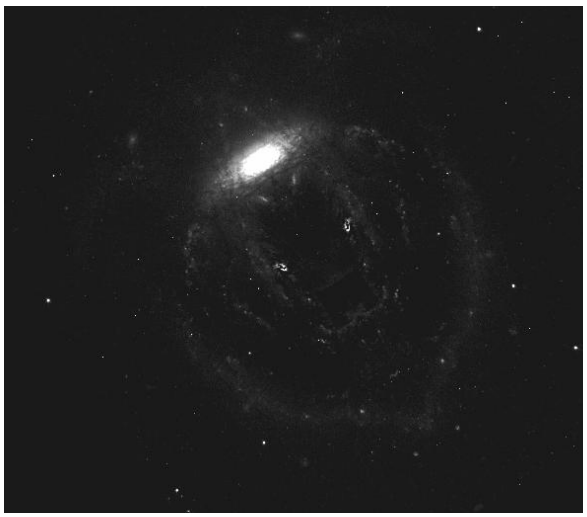

(f) Step 4: Rotate galaxy back into original plane

Figure 5.6: Exploiting symmetry to create transmission maps for background galaxy

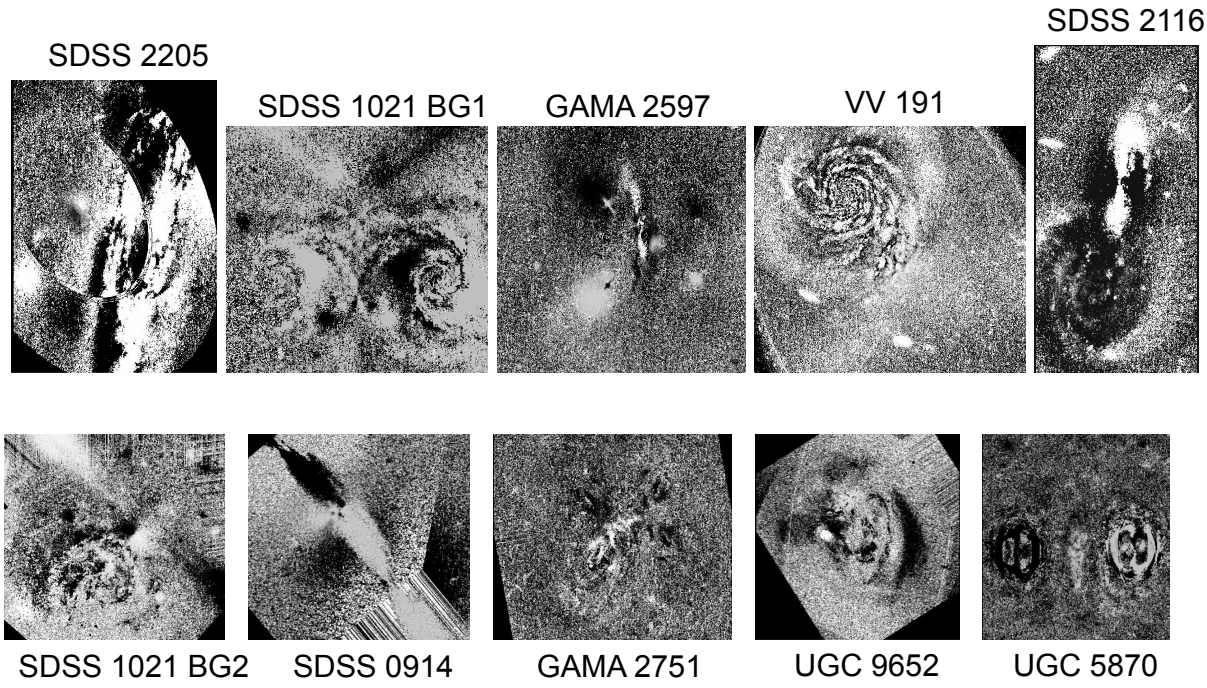

Figure 5.7: Transmission maps of all targets

ELLIPSE task failed to produce an accurate model, these values are less statistically significant. For the majority of the observations, however, we were able to use the generated table to deduce more about the foreground galaxy (the axial ratio, inclination, and scale length). We used the ELLIPSE-generated table and DS9 Imaging software to correct for the inclination angle of the foreground galaxy in order to estimate the distance from the foreground galaxy center to the backlit dust. The inclination corrections were done by stretching an ellipse fit about the features of the foreground spiral (e.g., spiral arms) into a circle. See Figure 5.8 for an example of the inclination corrections using UGC 9652. The yellow/green annuli represent how the image was stretched from the ellipse (in Figure 5.8a) to a circle in Figure 5.8b.

Once the emissions from both foreground and background galaxies had been divided out, and by effectively "zooming in" on the dusty region of the transmission maps, we isolated the dust in order to study its transparency and covering fraction. Again utilizing the table of values generated by the ELLIPSE task, we plotted transmission values as a function of the area of the dusty region where the listed fraction of the backlit area has transmission no greater than the listed value. Based on these plots we are able to make

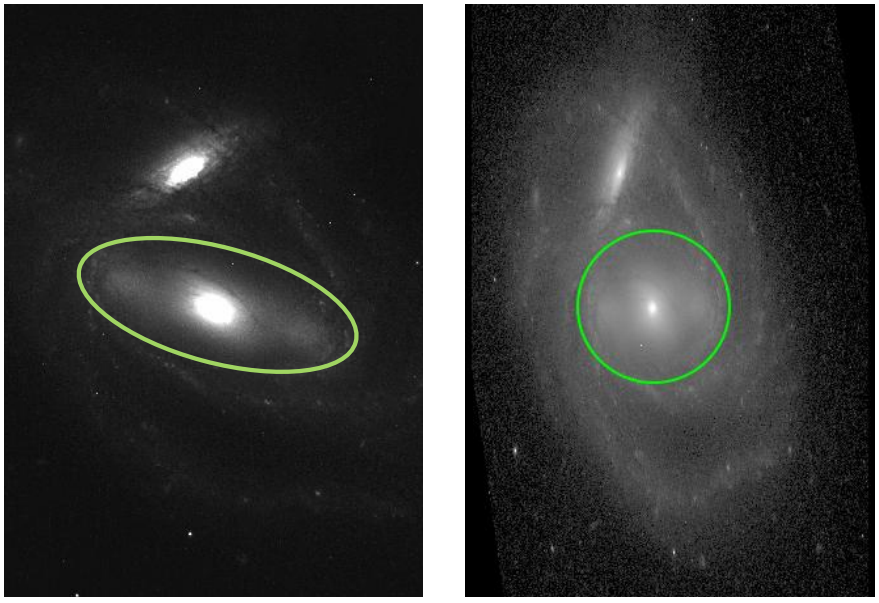

(a) UGC 9652 SNAPshot Image Before Inclination Corrections

(b) UGC 9652 Inclination Corrected Image

Figure 5.8: Example of Inclination Corrections Using UGC 9652

assumptions about the transparency of the dust in the isolated region and also gave us an idea as to the errors associated with each model. If we consider 100% of the isolated dust region, transmission should not exceed 1.0; anything above would be non-physical and is an indicator of combined random and systemic error levels.

CHAPTER 6
TARGET ANALYSIS

6.1 V005: UGC 9652

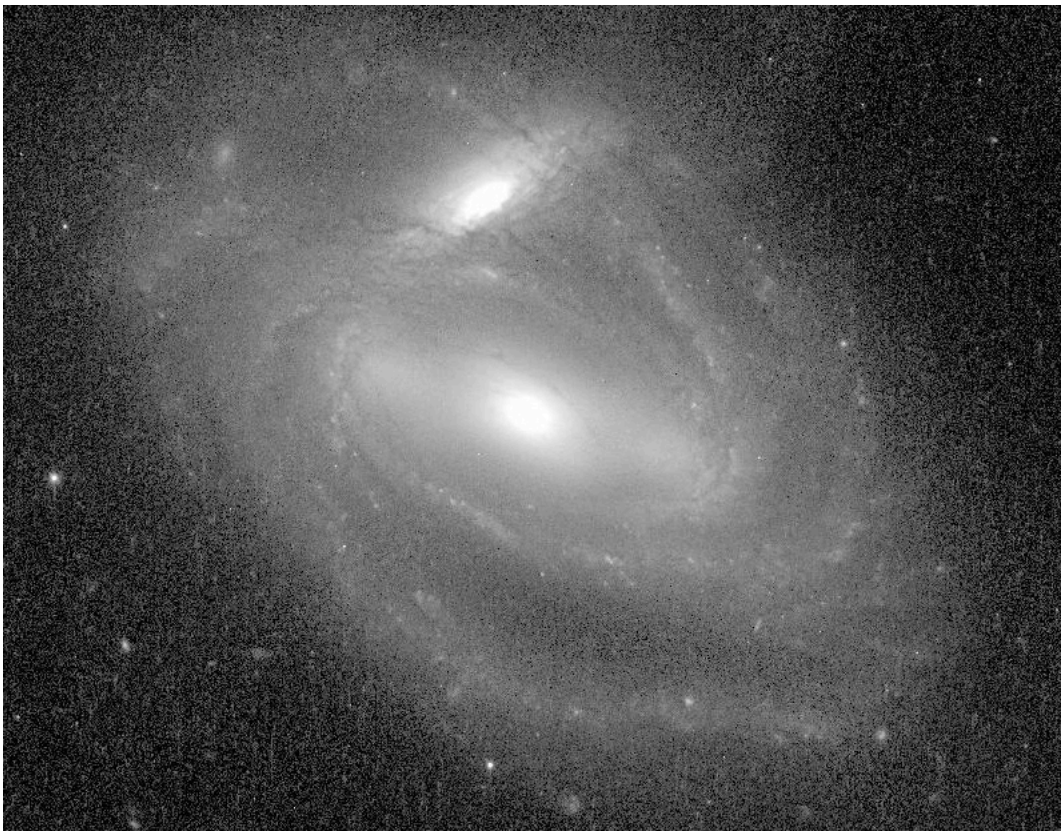

Figure 6.1: UGC 9652 SNAPshot image

This galaxy pair consists of an SB(r)c foreground spiral at redshift z=0.038 and an Sb background spiral at a redshift of z=0.074. The original SNAPshot image of the system, shown in Figure 6.1, shows a strong bar in the foreground spiral and two distinct regions of backlit dust in front of the background galaxy. The foreground galaxy has an estimated inclination of 63 degrees and a scale length of approximately 10 arcseconds.

From the HST SNAPshot images we noticed immediately that the background spiral nicely outlines the dust in at least two of the foreground spiral arms. The arms are

surrounded by nearly transparent "windows" where we see a variety of dust texture, where smooth dust manifests as flat residuals as our tests are not strongly sensitive to smooth dust (since big background galaxies do not allow us to see if there is enough smooth dust, while small background galaxy basically swallow it into their otherwise-unknown total brightness). In creating the transmission maps we first attempted to use the ELLIPSE task to isolate the backlit dust but because of the large bar in the foreground spiral galaxy, the isophote fitting failed to produce a reasonably accurate model. The task did however produce a sound model for the background and as a result we were able to effectively remove its emission from the image. We opted for using 2-fold symmetry about the X-axis to subtract the emission from the foreground galaxy. Based on this transmission map (see Figure 6.2, where the red box outlines the region of backlit dust) we were able to locate the dust out to roughly 21 arcseconds from the foreground nucleus. In this transmission map we notice a "web-like" distribution of the dust where not only does the dust follow the same orientation as the spiral arms but it also creates a basket weave pattern going perpendicular to the spiral arms. Figure 6.3 shows the transmission percentage for the backlit dust region as a function of area. Roughly 20% of the region has transmission over 1.0–an unphysical value–and is an indicator of the accuracy of the elliptical isophote model. This foreground galaxy is at least 50% transparent for more than 90% of the dusty region, is nearly transparent along the spiral arms, and appears to have transparent windows around its arm.

6.2 V014: SDSS 1021+17

This target group consists of a nearly face-on, 2-arm spiral galaxy of Hubble type Sc, and two background elliptical galaxies, shown in Figure 6.4. one of the background ellipticals is located "within" the inter-arm region of the foreground spiral (In reality of course, the background elliptical is too far away in redshift to actually be located within the spiral arm, but rather our perspective makes it appear as such). The dust appears to fan out along the spiral arms. There were several other galaxies in the HST SNAP-shot image, but their emission was either cropped out or masked in order to minimize

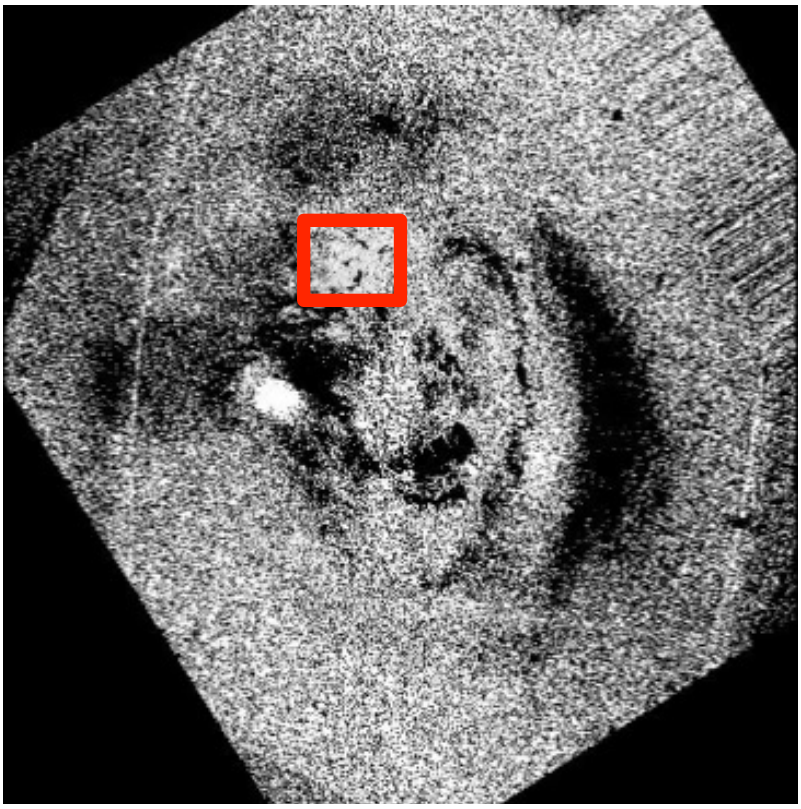

Figure 6.2: UGC 9652 Transmission Map

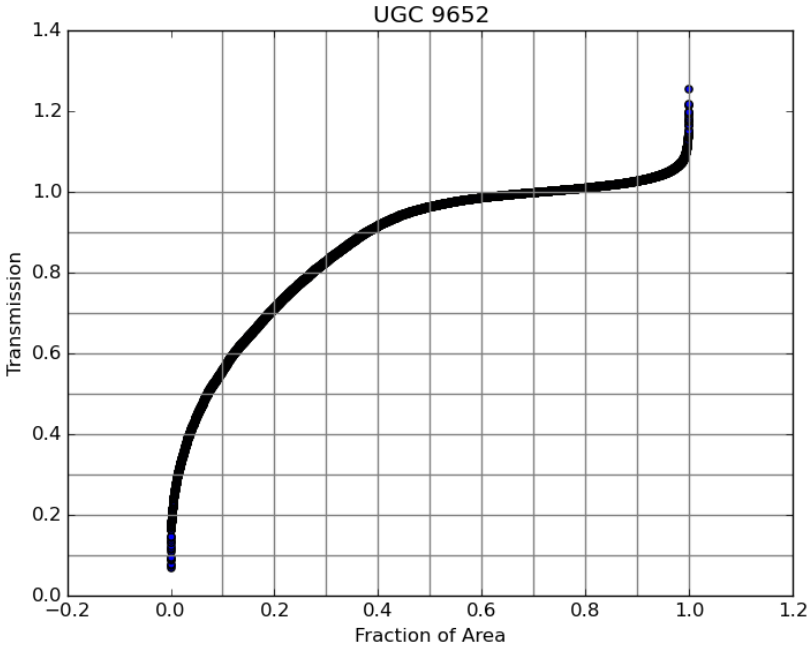

Figure 6.3: UGC 9652 Transparency Plot

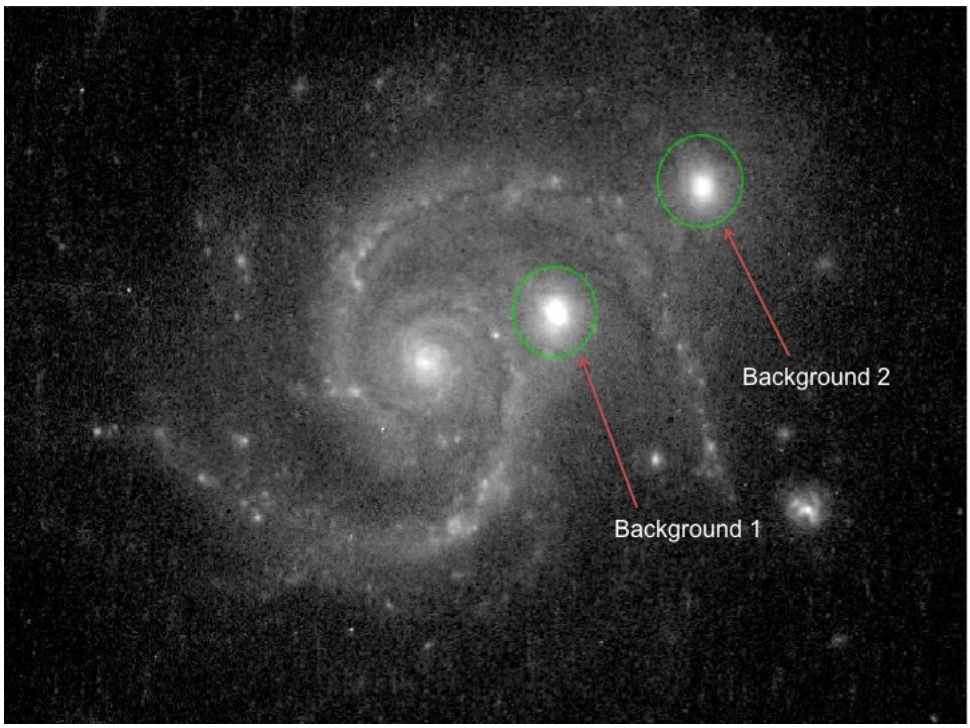

Figure 6.4: SDSS 1021 SNAPshot Image

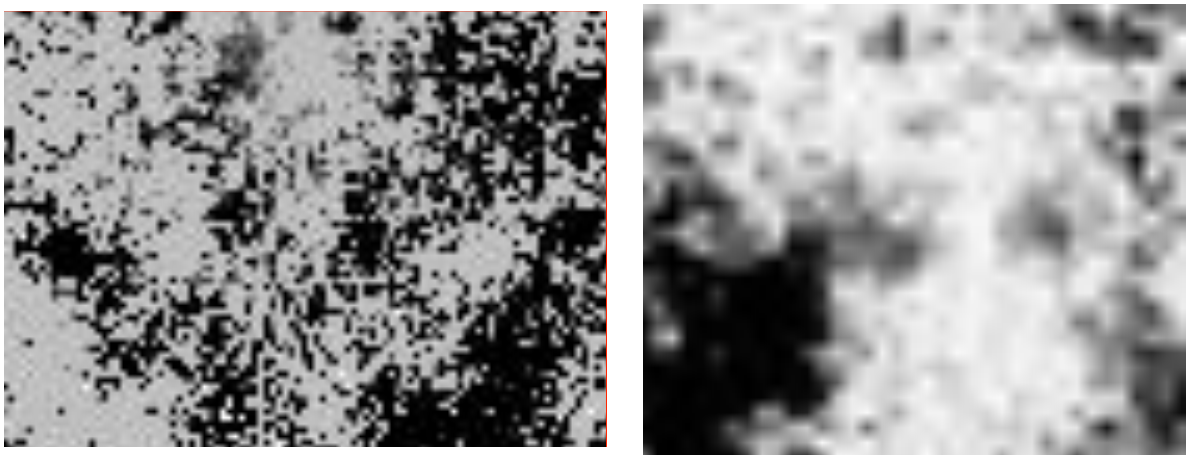

(a) SDSS 1021 Background 1

(b) SDSS 1021 Background 2

Figure 6.5: SDSS 1021 Transmission Maps

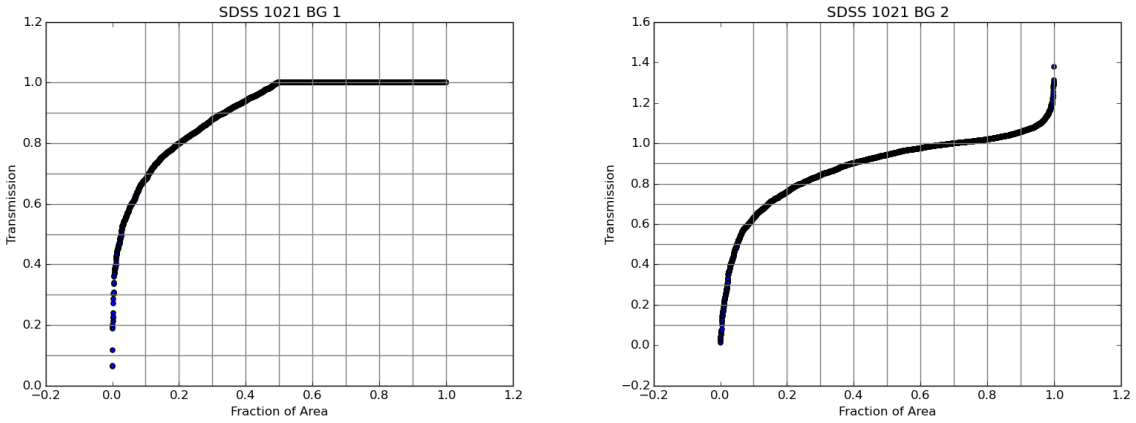

(a) SDSS 1021 Background 1 (b) SDSS 1021 Background 2

Figure 6.6: SDSS 1021 Transparency Plots

their contribution. We used rotational symmetry to first remove the emission from the foreground spiral then used reflection symmetry on each of the background ellipticals to produce two transmission maps, shown in Figure 6.5 where again the red areas indicate the regions of backlit dust. Because of the location of each of the elliptical galaxies (one in the inter-arm region and one outside the spiral arms), we are given a unique opportunity to investigate how far in radius the dust lies from the center of the spiral. We see very little backlit dust near the elliptical outside of the spiral, implying the majority of the dust lies closer in radius. In the inter-arm region however, we again see the web-like pattern where while some of the dust follows the spiral arms and some actually appears perpendicular to the arms. For this study, the background galaxy located outside the spiral arms is called "background 1" and the background elliptical located within the inter-arm region has been named "background 2". After inclination corrections, the backlit dust in front of background 1 is estimated to be approximately 9 arcseconds away from the foreground nucleus, and approximately 4 arcseconds separate the nucleus from the backlit dust in front of background 2. In looking at the transmission for background 1, it appears that nearly 50% of the transmission area is transparent whereas for background 2, located in the inter-arm region, the transmission is transparent for only 30% of the dusty region. Both plots can be seen in Figure 6.6

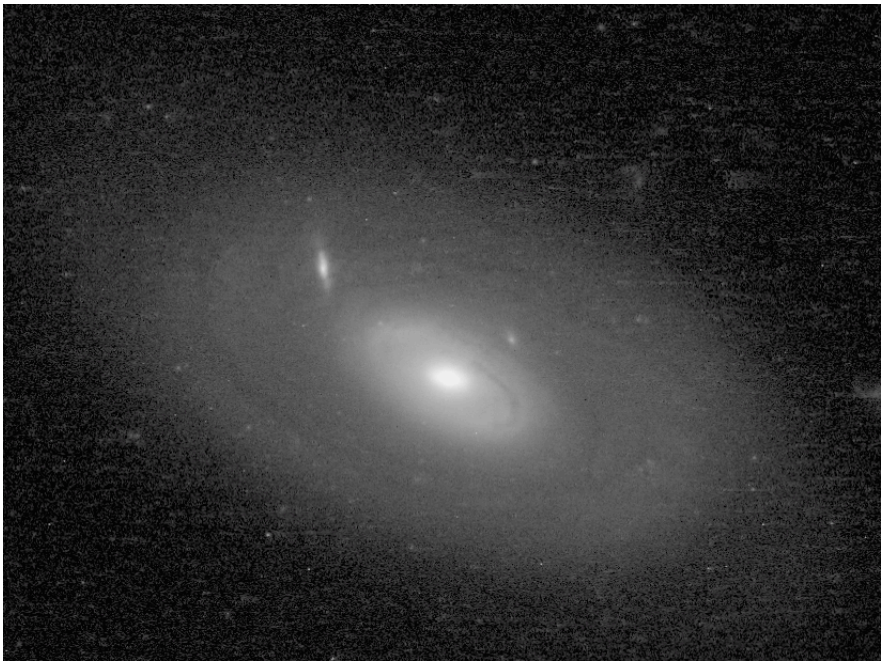

Figure 6.7: GAMA 2571 SNAPshot Image

6.3 V016: GAMA 2751

This system includes two galaxies which are the most spatially separated of all the targets considered in this study. The foreground galaxy is of Hubble type Sab and is at a redshift of z=0.0421. The background galaxy is located at redshift z=0.29. For this system we first created an isophote model of the foreground galaxy and then used a median filter to smooth the model before subtracting it away from the original image. We used 4-fold reflection symmetry to divide out the emission of the background galaxy. The resulting transmission maps show two dust lanes that appear to follow the orientation of the foreground galaxy, and one that crosses perpendicularly between them as if to form the letter "H". By looking at the image, the perpendicular contribution was determined to be a dust lane of the background galaxy and not associated with the dust structure seen in the foreground. We estimate the dust to be approximately 6-7 arcseconds away from the foreground nucleus. The dust structure of these systems is very opaque for roughly 1/3 of the dusty region and jumps up suddenly in transparency before continuing to rise linearly for the remainder of the region.

Figure 6.8: GAMA 2751 Transmission Map

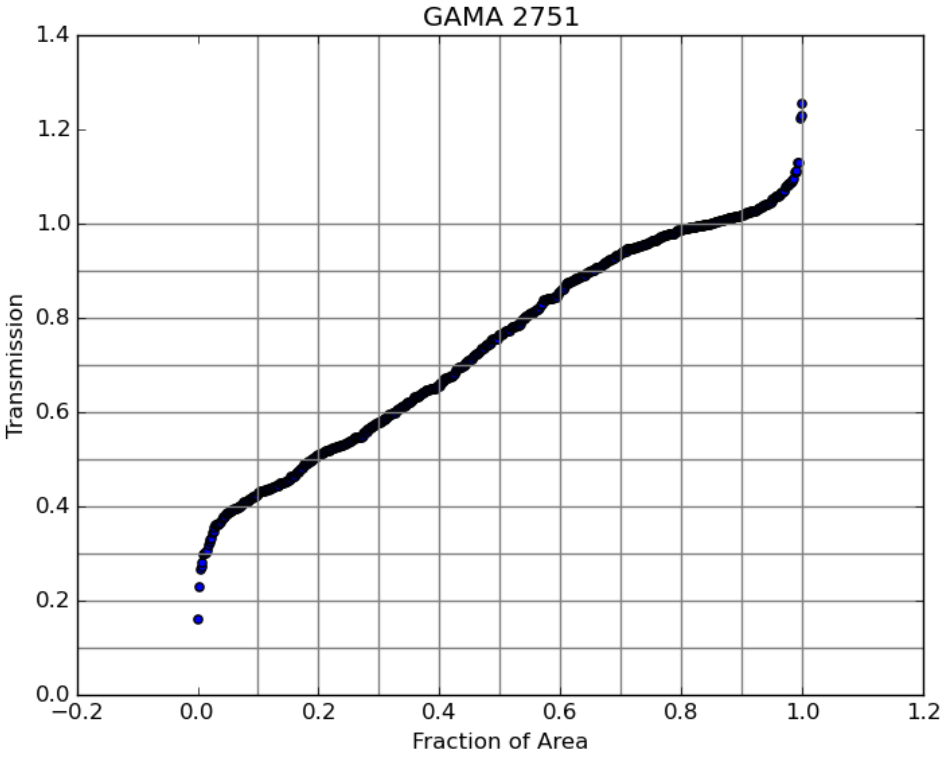

Figure 6.9: GAMA 2751 Transparency Plot

6.4 V022: GAMA 2597

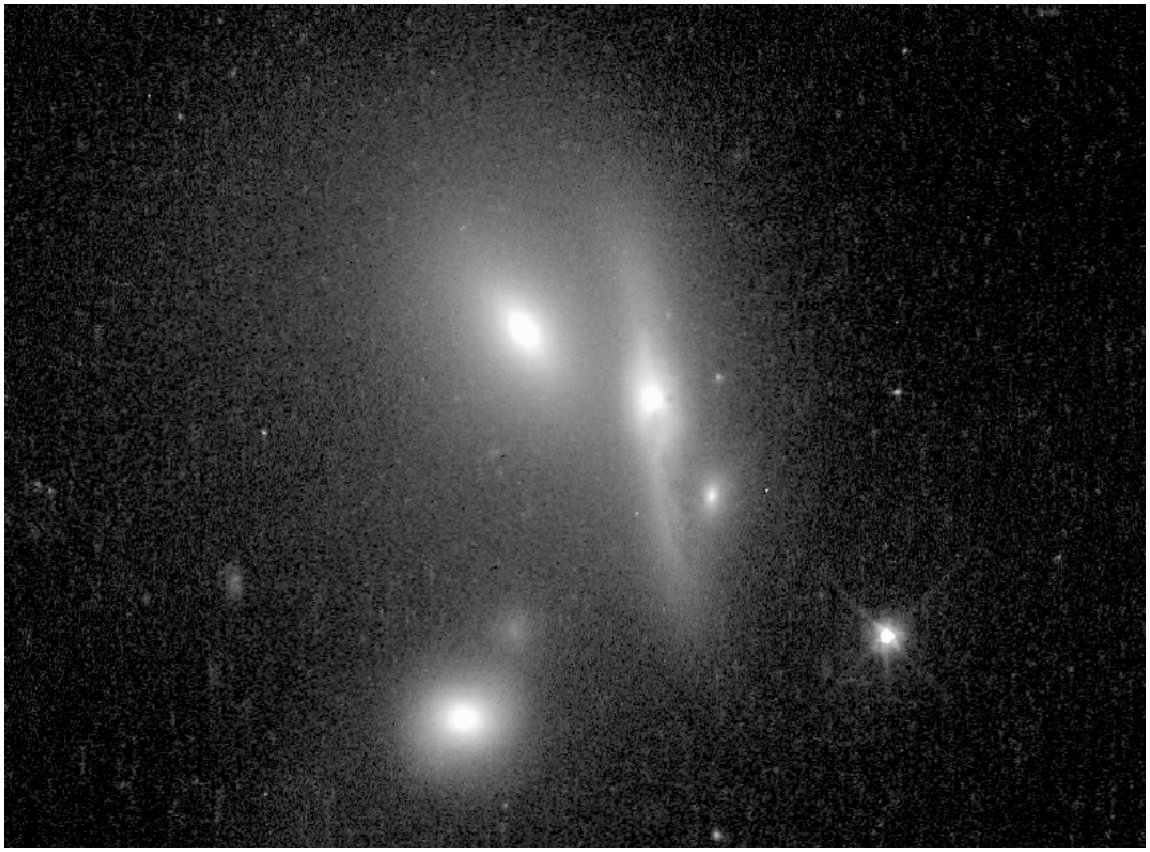

Figure 6.10: GAMA 2597 SNAPshot Image

This pair of galaxies features a thin spiral disk and appears to have filamentary dust structure which is backlit on one half of the disk by the background galaxy. The dwarf-ish galaxy is a lot like the one found serendipitously in HST data for the ACS Nearby Galaxy Survey (see Holwerda et al., 2009, 2013). The dust appears only on one side of the foreground nucleus and does not appear to have a counterpart on the opposite side. This system is about as opaque as we can measure. The elliptical isophote fit used to model the foreground required a median filter to smooth out the areas around the location of the dust, but overall produced an accurate model despite the galaxy's near edge-on appearance. We used 2-fold reflection symmetry about the Y-axis to divide out the emission from the background. The dust structure seen in the transmission maps ranges from 2 to 4 arcseconds away from the foreground nucleus and appears to follow the dust lanes seen throughout the thin disk of the foreground galaxy. There does not appear to be the same web-like dust structure as seen in other systems. Over 50% of

Figure 6.11: GAMA 2597 Transmission Map

the dusty region has no transmission, while 20% of the region has a transmission greater than 1.0. We notice the absence of an inflection point in the transmission plot that is present in all but one of the other targets.

6.5 V031: SDSS 0914+49

The foreground spiral in this system has less defined spiral structure (could be considered "flocculent") but has very prominent dust structure throughout the disk. This Scd galaxy is at a redshift of z=0.0345 and the corresponding background galaxy is at redshift z=0.1194. In this system we see thick, winding dust lanes with a well-defined edge. While the elliptical isophote fitting for the foreground galaxy wasn't ideal because of the galaxy's inclination, the problem areas associated with the fit were concentrated in the inner portions of the spiral disk and not within close proximity to the backlit dust, thereby allowing us to use the isophote fitting to divide out the emission within the dusty region. 2-fold reflection symmetry about the Y axis was used to divide out the emission of the background galaxy. The dusty region, located nearly 11 arcseconds from the fore-

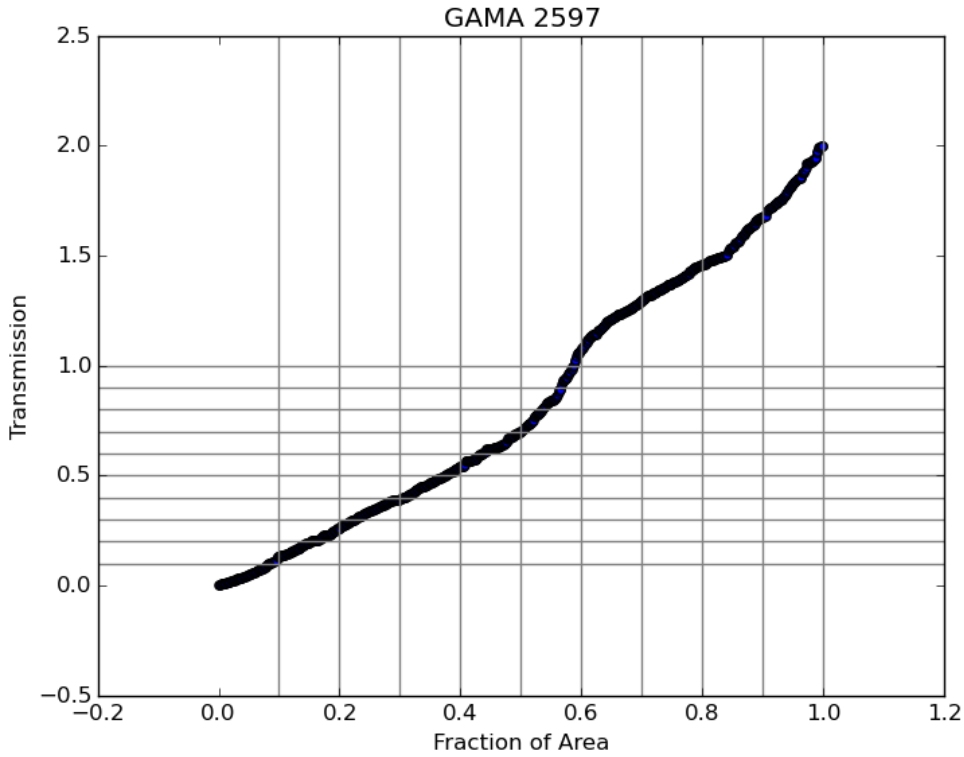

Figure 6.12: GAMA 2597 Transparency Plot

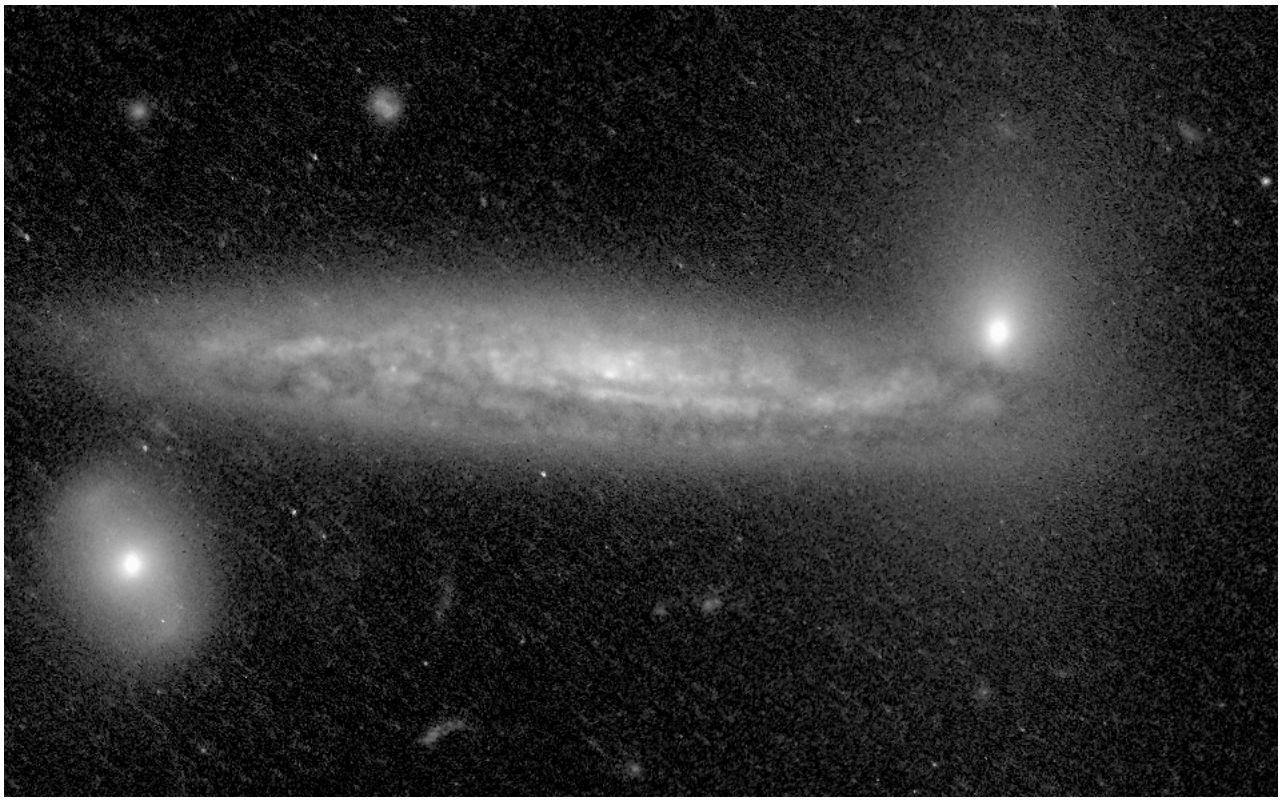

Figure 6.13: SDSS 0914 SNAPshot Image

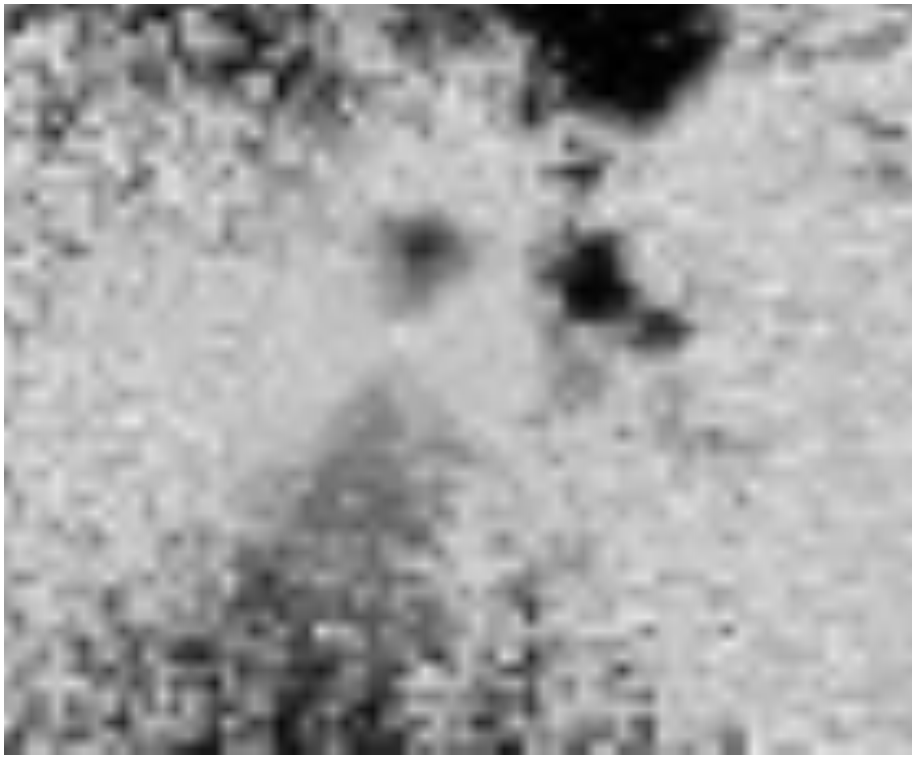

Figure 6.14: SDSS 0914 Transmission Map

ground nucleus, again seems to have a sharp divide in transparency: approximately 25% of the region is completely opaque whereas the other 75% of covered area has at least 45% transparency. In this target system, 20% of the transmission values were over 1.0.

6.6 V037: SDSS 2205-00

This galaxy pair includes an SB(?)(r)bc spiral galaxy at redshift z=0.0311 and background galaxy at z=0.1445. We see a dust lane and patch of dust within approximately 9 arcseconds from the foreground galaxy and nothing outside of that radius. Unfortunately for this target system, neither elliptical-isophote fitting nor symmetry produced adequate models for the foreground galaxy- a not entirely surprising result given its high inclination. We measured the distance to the dust from the foreground nucleus after making inclination corrections to the image and determined the dust to exist approximately 9 arcseconds from the foreground nucleus. The dusty region has no sign of the same web-like structure in the dust seen in other spirals of this survey, but if the trend of the transmission plot is assumed to be accurate, at the radius of the dust the foreground

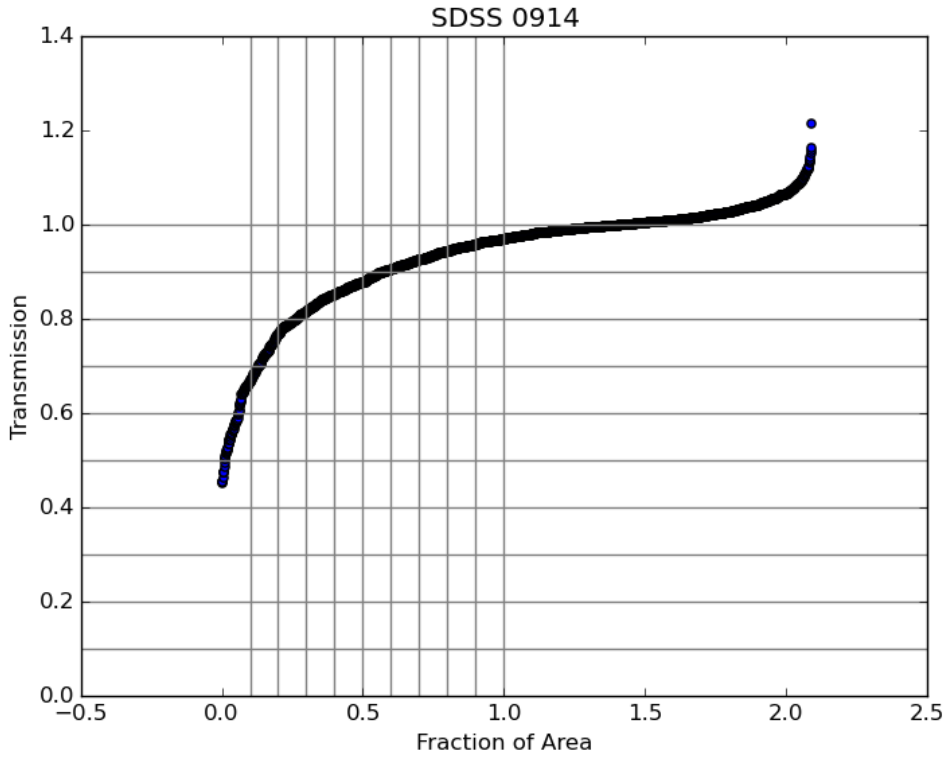

Figure 6.15: SDSS 0914 Transparency Plot

galaxy appears to be reasonably transparent.

6.7 V039: VV 191

This pair of galaxies is the ideal target system for the occulting-galaxy approach because the foreground Sc spiral is nearly face-on and partially overlaps a background elliptical galaxy. While their redshifts are closer together than was required to be a target for the survey, there is no indication that the two galaxies are interacting. The emission from the foreground spiral was removed by using 180-degree rotational symmetry while the emission from the background was divided out nicely with its corresponding elliptical-isophote model. The transmission map shows dust structure that contrasts the orientation of the spiral arms, again in a "web-like" pattern. The transmission plot shows the steep jump in transmission from completely opaque for nearly 35% of the dusty region to at least 50% transmission for the remaining area, and an inflection point where the transmission levels off before reaching complete transparency. Because of the geometry

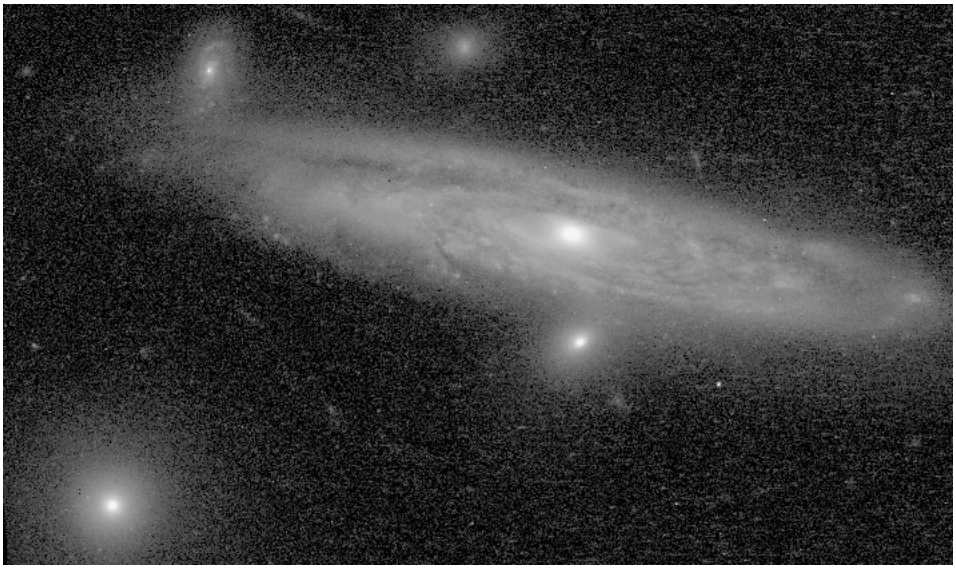

Figure 6.16: SDSS 2205 SNAPshot Image

of this target system, we're given a unique opportunity to study the radius at which the dust exists. The backlit dust in this system is located approximately 18 arcseconds from the foreground nucleus but beyond that radius we see no dust at all- creating a strict boundary approximately 1.4 Petrosian radii from the foreground. If the dust were to exist outside that boundary, the position of the background elliptical would allow us to observe it.

6.8 V042: UGC 5870

This galaxy pair consists of a nearly face-on SB(r)bc spiral galaxy at redshift z=0.0068 and a background galaxy at redshift z=0.0444. From just the HST SNAPshot images alone, the backlit dust is extremely prominent along the entire length of the background galaxy and creates a web-like pattern across its emission. Because of the strong bar in the foreground spiral, the ellipse fitting for the inner region of the spiral was poor, even when a median filter was applied to patch over the affected area. The backlit dust, however, was unaffected given its location far from the center of the foreground. We used 4-fold symmetry to divide out the transmission of the background galaxy and were left with a map of the dust structure which seems to follow the web-like pattern observed in other systems. Not only does the dust seem to follow the spiral structure of the foreground,

Figure 6.17: SDSS 2205 Transmission Map

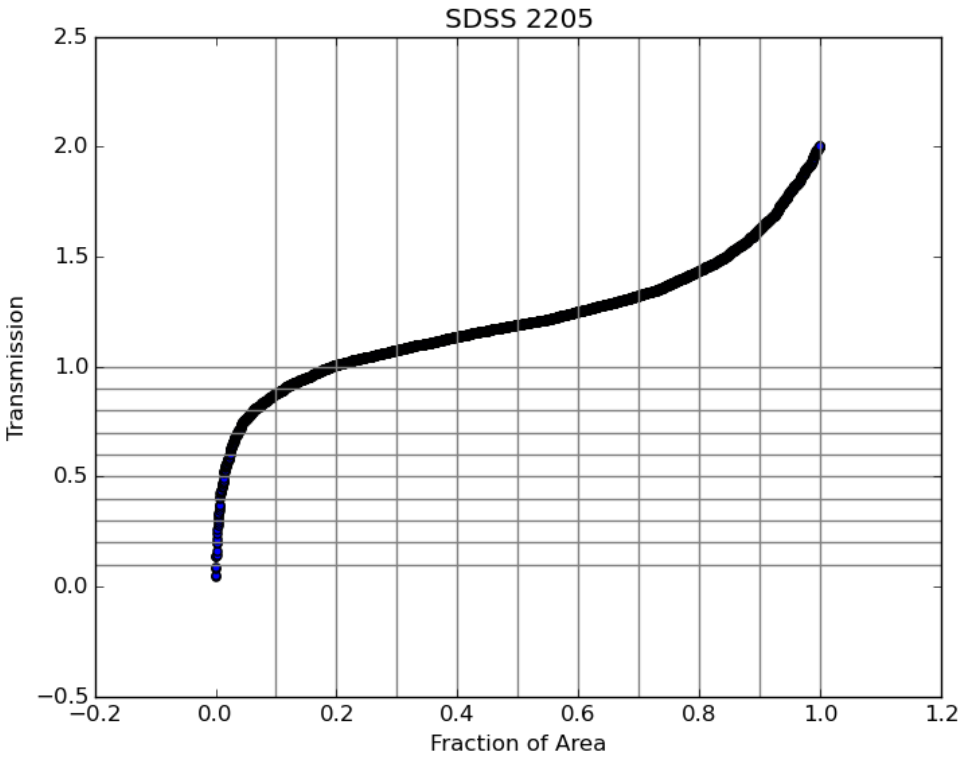

Figure 6.18: SDSS 2205 Transparency Plot

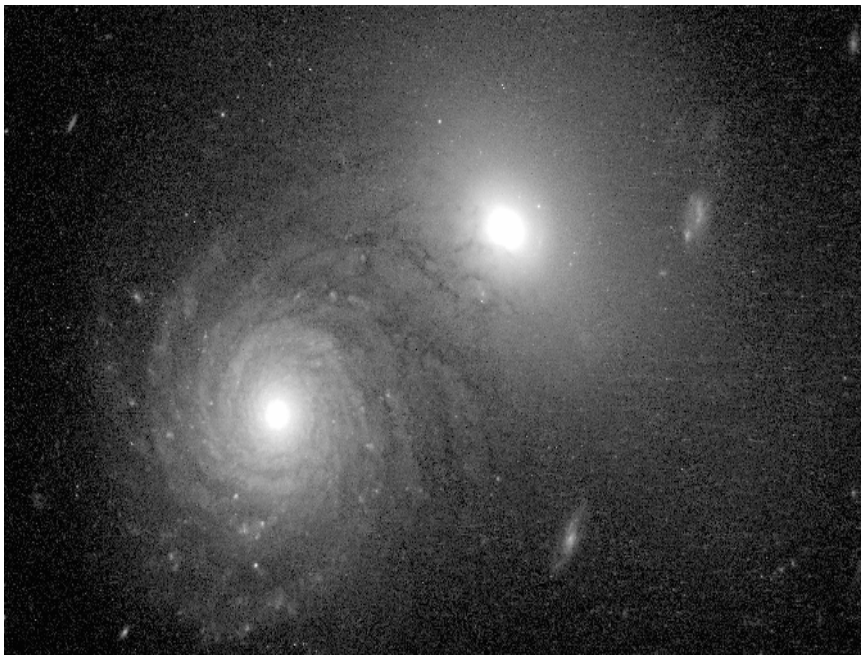

Figure 6.19: VV 191 SNAPshot Image

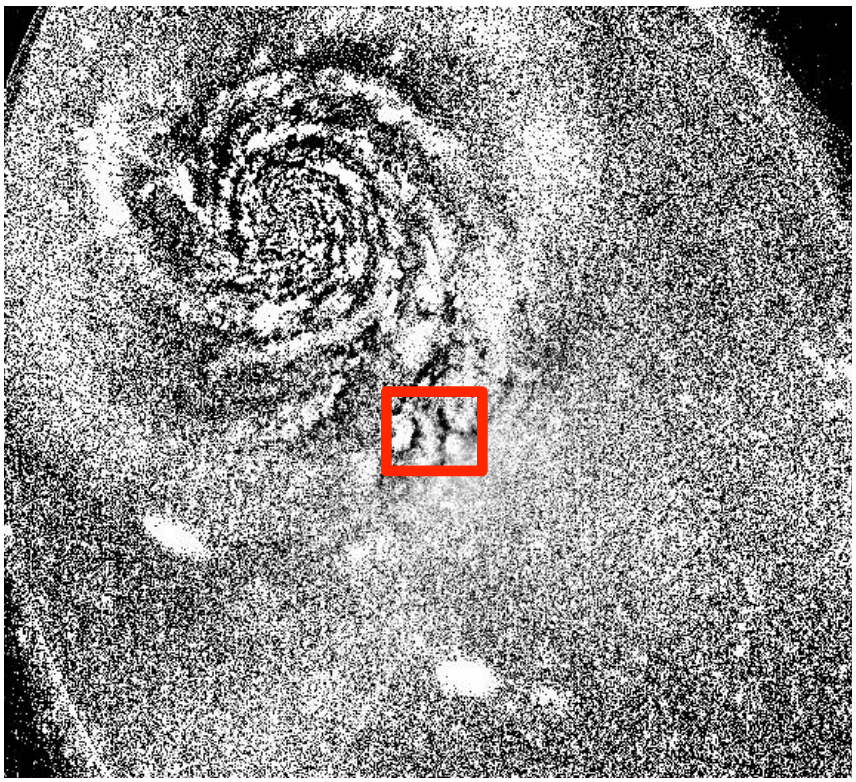

Figure 6.20: VV 191 Transmission Map

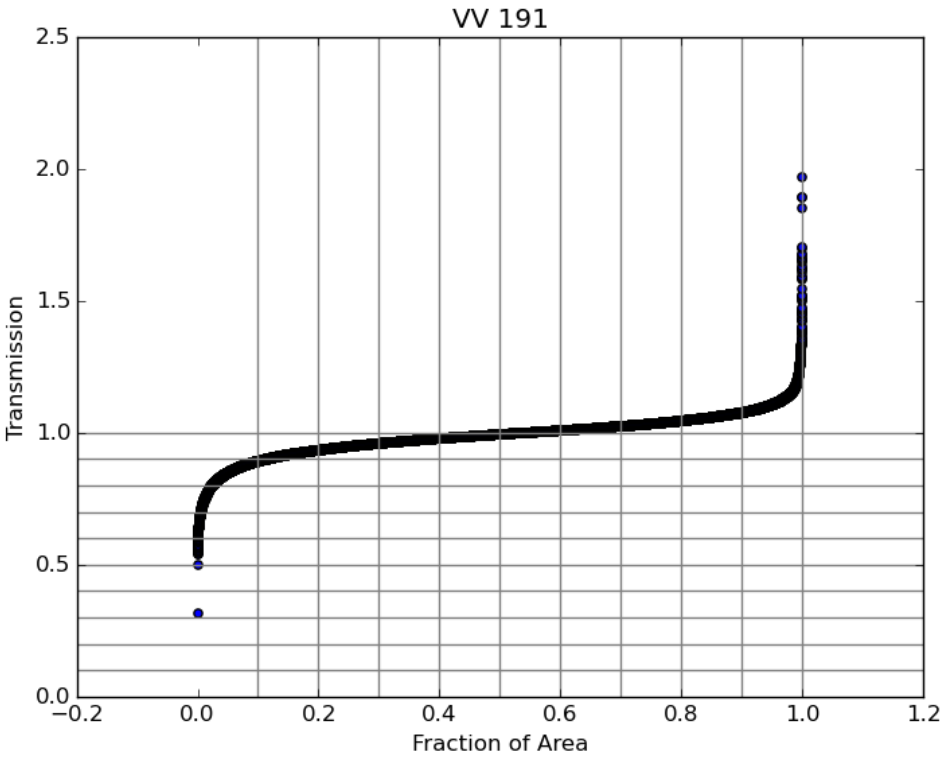

Figure 6.21: VV 191 Transparency Plot

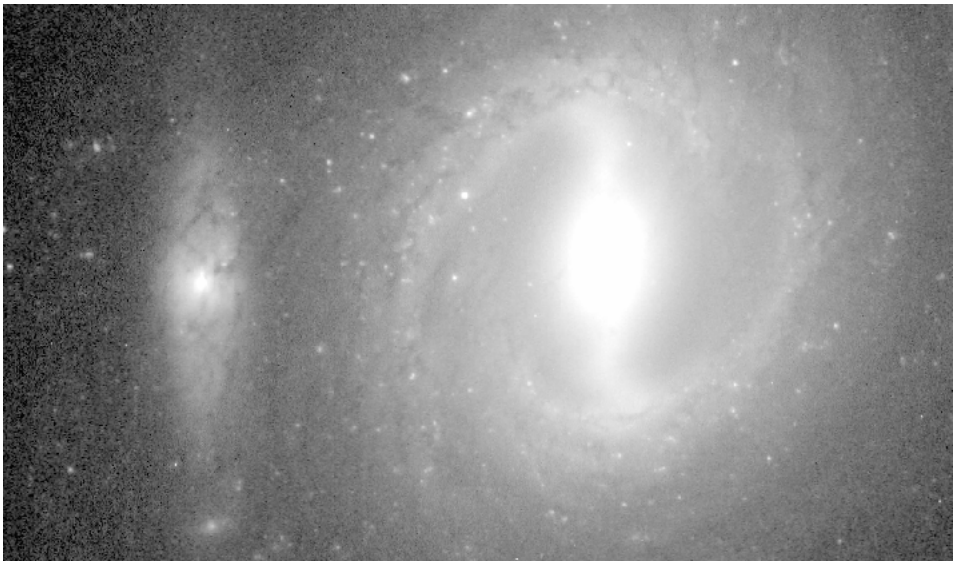

Figure 6.22: UGC 5870 SNAPshot Image

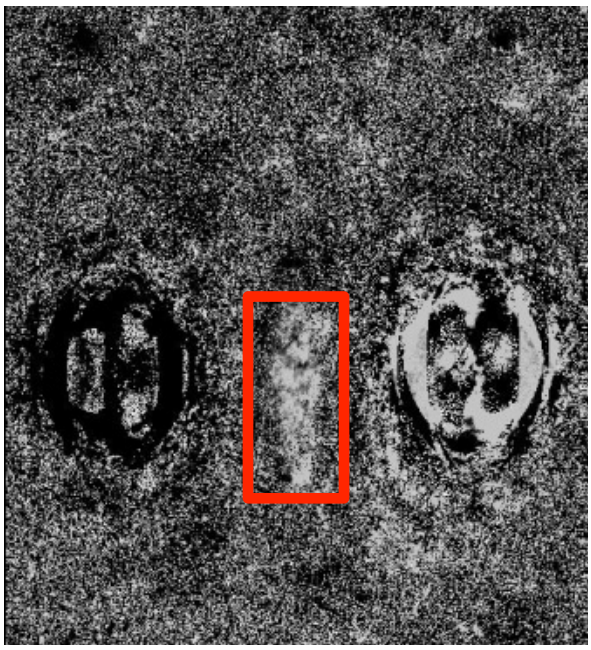

Figure 6.23: UGC 5870 Transmission Map

but there is also structure perpendicular to the arms. Here we see a nearly linear rise in transparency: 20% of the covered area being completely opaque and another 20% completely transparent, the remaining 60% being somewhere in between.

6.9 V045: SDSS 2116+00

This target system includes a SB(r)c foreground galaxy at redshift z=0.0318 and a background spiral galaxy at redshift z=0.0439. We used 180-degree rotational symmetry of the background galaxy which included the uses of a median filter to suppress star-forming knots in the spiral arms. The elliptical-isophote technique was used on the foreground to divide out its emission. The dusty region spanned a wider range of radii from the foreground spiral although no web-like pattern was observed in the dust. The dusty region spanned a total of 6 arcseconds: between 8 and 14 arcseconds from the foreground nucleus. The transmission plot, like visit 22 (V022), shows no inflection point- a feature not absent in the other plots, and shows that over 80% of the dusty region is optically thin.

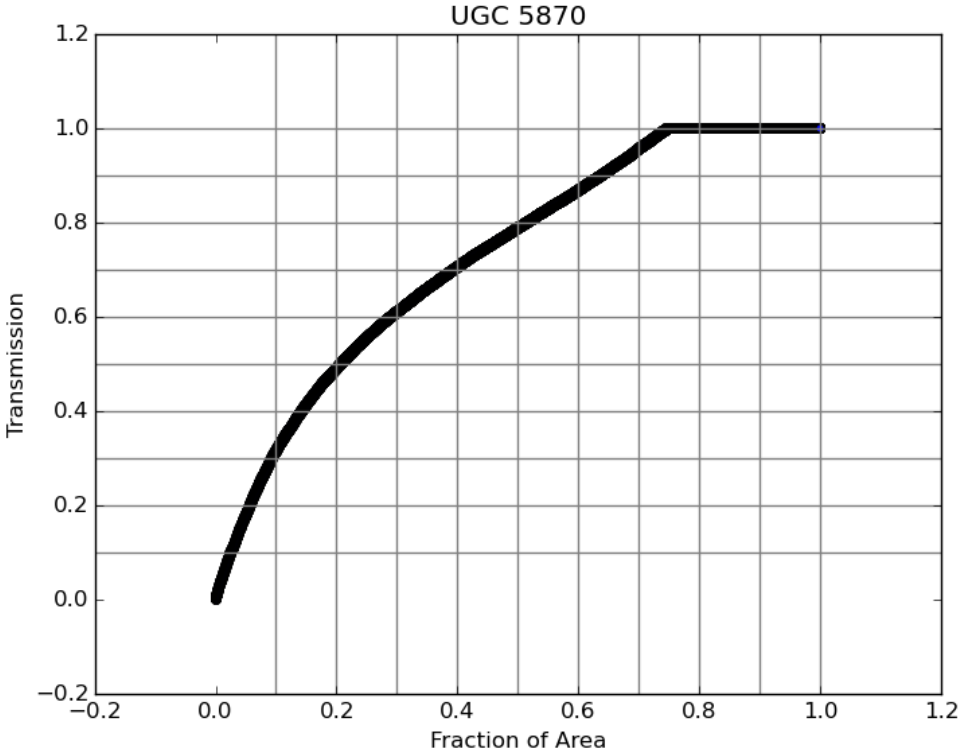

Figure 6.24: UGC 5870 Transparency Plot

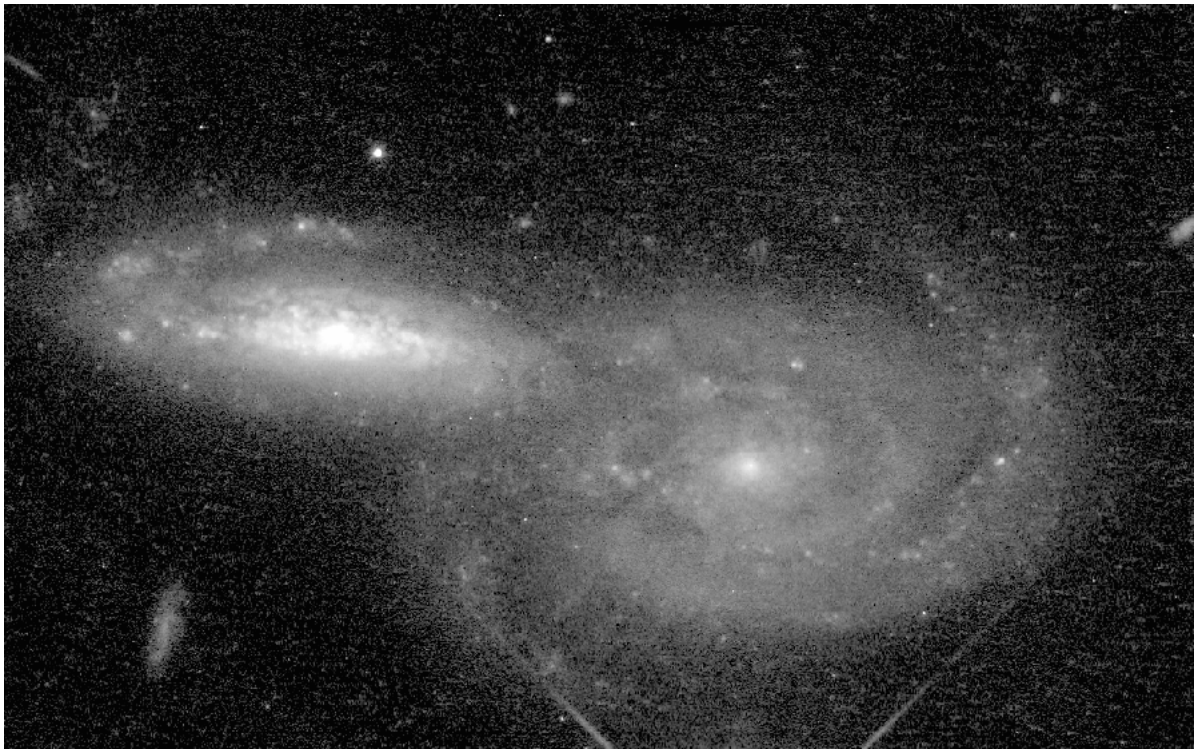

Figure 6.25: SDSS 2216 SNAPshot Image

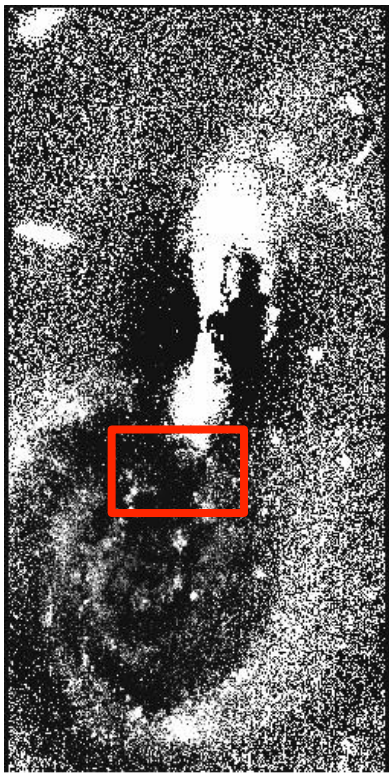

Figure 6.26: SDSS 2116 Transmission Map

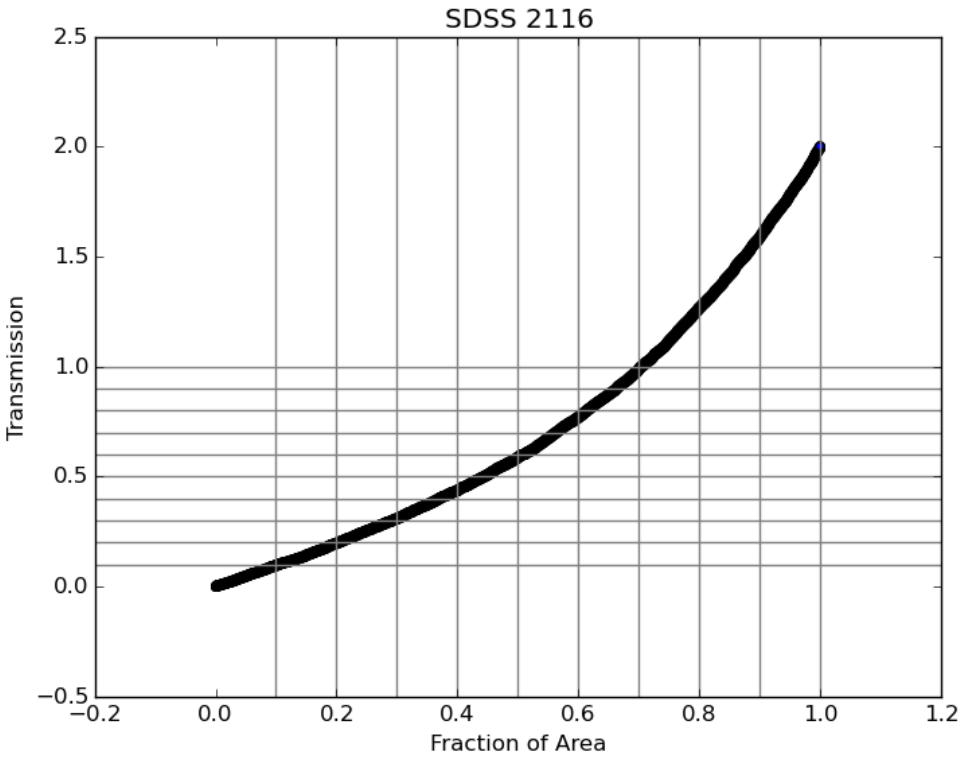

Figure 6.27: SDSS 2116 Transparency Plot

CHAPTER 7

ANALYSIS

The transmission maps produced in this study allowed us to investigate the dust structure in foreground galaxies within the backlit region, including how the dust in the region is structured and distributed. Given the early debate about the opacity of spiral galaxies, we also used the transmission maps to analyze the transparency of the targets within the sample. Finally, we looked at physical characteristics (i.e., Hubble type, star formation rates, mass, etc) of each target in order to draw statistically-relevant conclusions about the dust within the backlit region of the foreground galaxies.

As a quick reference, we've included a summary of our analysis results in table 7.1 including the average distance from foreground nucleus to the backlit dust region in both arcseconds and as a function of Petrosian radius, and whether or not we are able to identify a "web-like" pattern in the dust structure, or if there is a visible edge to the dust structure (the details of such are discussed below).

7.1 Web-like Structure

It makes sense intuitively, and is the dominant structure seen in optical images of spiral galaxies, for dust lanes to follow the pitch angle of the spiral arms. For three targets in this sample however, we found that no only does the dust follow the pitch angle, but it also appears at various other angles, creating a "web-like" pattern in the dust structure. This existence of the structure is not necessarily new (a simple Hubblesite.org search within the galaxies picture gallery will show several other examples of the phenomenon) but what is interesting is that based on our analysis of the transmission maps, the "web-like" pattern is only present in late-type foreground galaxies, specifically of Hubble type SBc/Sc/Sbc. VV 191, which includes a foreground galaxy of Hubble type Sc, is shown in

Object	Distance from FG nucleus to backlit dust (arcsec)	Distance from FG nucleus to backlit dust (Pet_Rad)	Web?	Edge Visible?
UGC 9652	21.36 35.53	0.96 1.60	yes	no
SDSS 1021 BG 1	9.37	0.93	no	no
SDSS 1021 BG 2	4.10	0.41	yes	no
GAMA 2751	6.76	0.88	no	no
GAMA 2597	2.10 4.57	0.17 0.38	no	no
SDSS 0914	10.92	0.67	no	yes
SDSS 2205	9.45	0.47	no	yes
VV 191	18.87	1.39	yes	yes
UGC 5870	16.18	1.21	yes	no
SDSS 2116	7.92 13.77	0.57 1.00	no	no

Table 7.1: Analysis Summary from Transmission Maps

Figure 7.1. The original SNAPshot image of VV 191 is presented in Figure 7.1(a), where the circle indicates the region of backlit dust analyzed in the transmission map, which is shown in Figure 7.1(b). The arrows in Figure 7.1(b) indicate the dust lanes that appear nearly perpendicular to the pitch angle of the spiral arms. We were able to identify the same "web-like" pattern in three other systems: SDSS 1021Background 2 (Hubble type Sc), UGC 5870 (Hubble type SB(r)bc), and UGC 9652 (Hubble type SB(r)c). Figures 7.2, 7.3, and 7.4 all include the original SNAPshot image of SDSS 1021, UGC 5870, and UGC 9652, respectively, with a circle indicating the region of backlit dust analyzed in the transmission map, and the transmission maps with arrows indicating the dust lanes which do not appear to follow the pitch angle of the spiral arms.

7.2 Edge of Dust

In systems of optimal geometry, we were able to identify a strict radial limit to the dust structure in the foreground spiral galaxy. The dust in these systems has a clear maximum radius, beyond which we see no dust. In two of the three cases (SDSS 0914 and SDSS 2205), this "optimal geometry" involved systems with high inclination. The

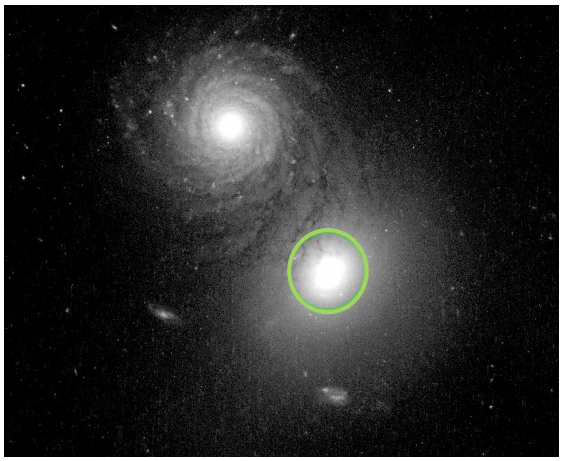

(a) VV 191 Original SNAPshot Image

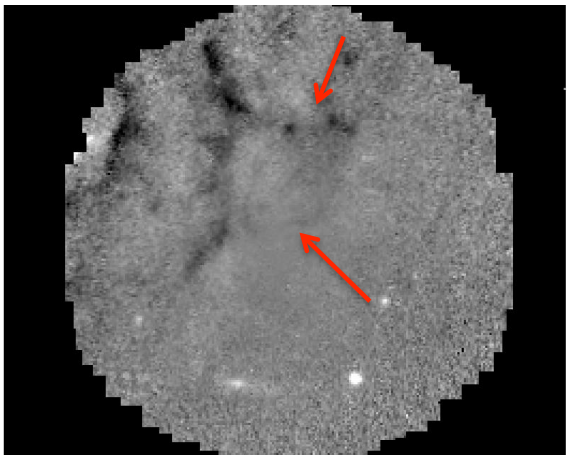

(b) Web-like Dust Structure in Transmission Map

Figure 7.1: VV 191: Evidence of web-like dust structure within backlit region

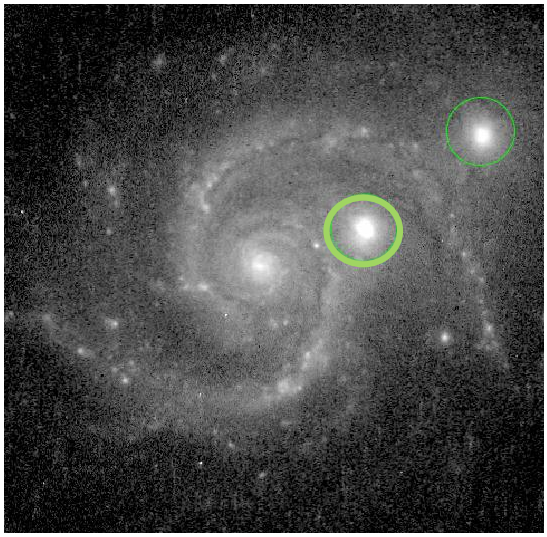

(a) Original SNAPshot Image of SDSS 1021 Background 2

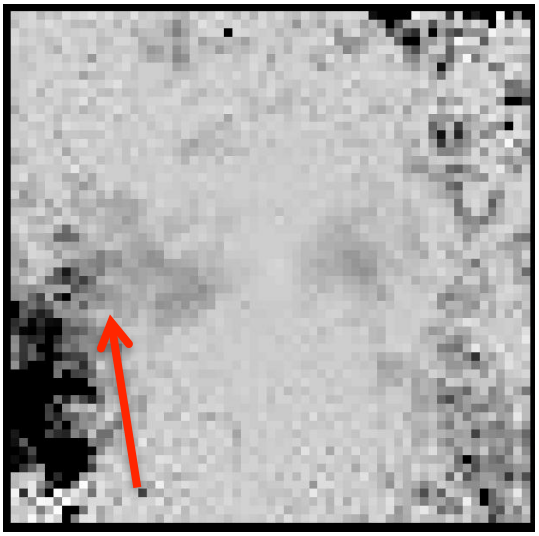

(b) Web-like Dust Structure in Transmission Map

Figure 7.2: SDSS 1021: Evidence of web-like dust structure within backlit region

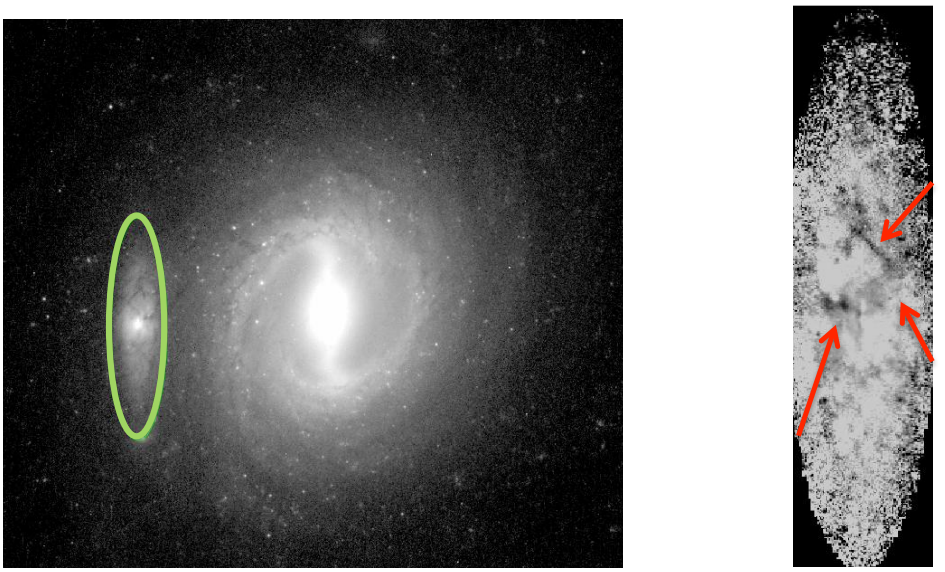

(a) Original SNAPshot Image of UGC 5870

(b) Web-like Dust Structure in Transmission Map

Figure 7.3: UGC 5870: Evidence of web-like dust structure within backlit region

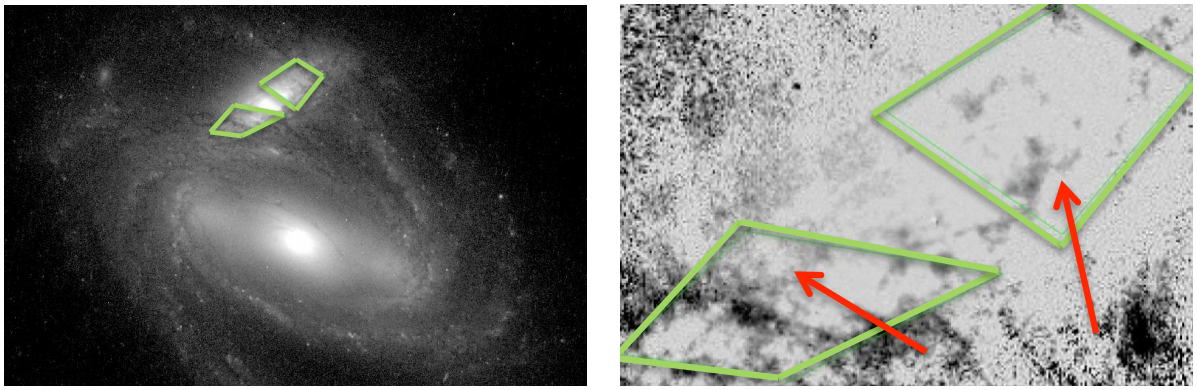

(a) Original SNAPshot Image of UGC 9652

(b) Web-like Dust Structure in Transmission Map

Figure 7.4: UGC 9652: Evidence of web-like dust structure within backlit region

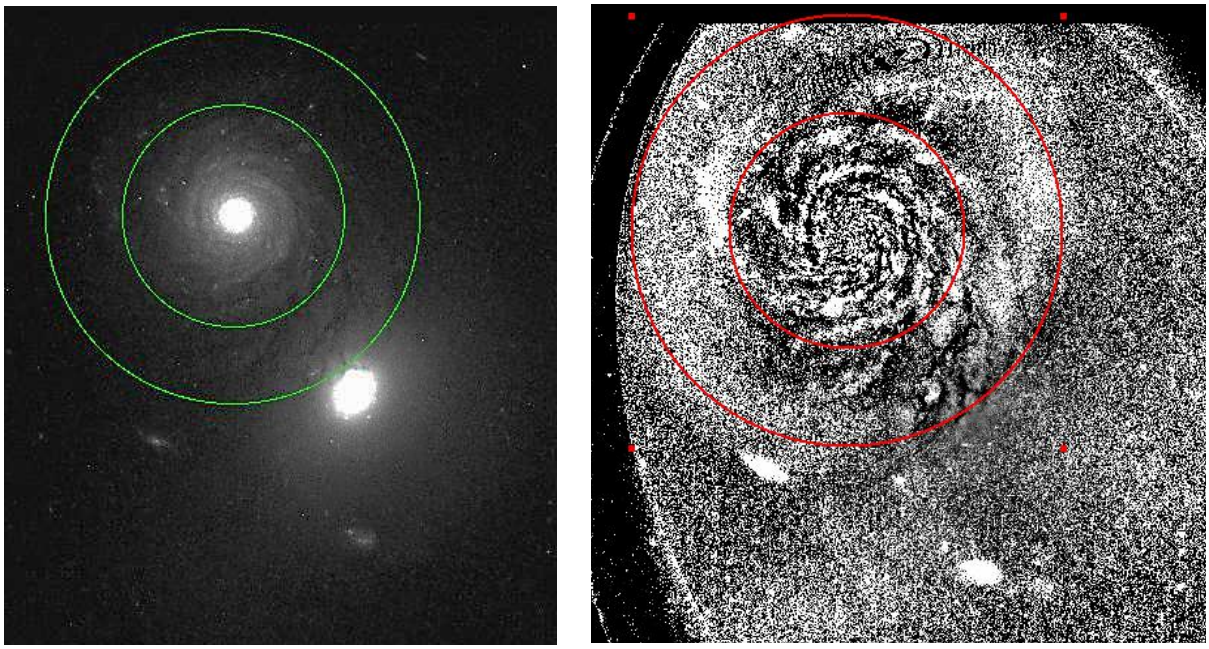

(a) Original SNAPshot Image of VV 191 (b) Transmission Map of VV 191

Figure 7.5: VV 191: Edge of dust structure from the SNAPshot image and dust map

third case, VV 191, involved a nearly face-on system with a background galaxy that is far enough (radially) from the foreground nucleus analyze the distinct edge. VV 191 was the most interesting of the three because the backlit region of dust used to create the transmission maps included the furthest edge of the dust structure. The transmission map clearly shows just how strict and distinct this radial limit appears. Additionally, because of the backlit dust we are able to see that the dust within the foreground spiral actually continues out far beyond what might have been the estimated limit to the galaxy had the background galaxy not existed. Quantitatively speaking, the foreground spiral in VV 191 appears approximately 1.7 times larger in attenuation as its dust lanes do against its own light, or its starlight in the HST data. The outer annuli in Figures 7.5(a) and 7.5(b) identify the strict limit of observed dust structure in both the original SNAPshot image and transmission map, respectively. The inner annulus represents what may have been the (naively) assumed radial limit to the foreground galaxy had the background not illuminated further dust structure.

The other two examples of this maximum radius in the dust structure were observed in the highly inclined systems of SDSS 0914 and SDSS 2205. The annuli in figures 7.6(b) and 7.7(b) indicate the edge of the dust structure as seen in these two targets. While less

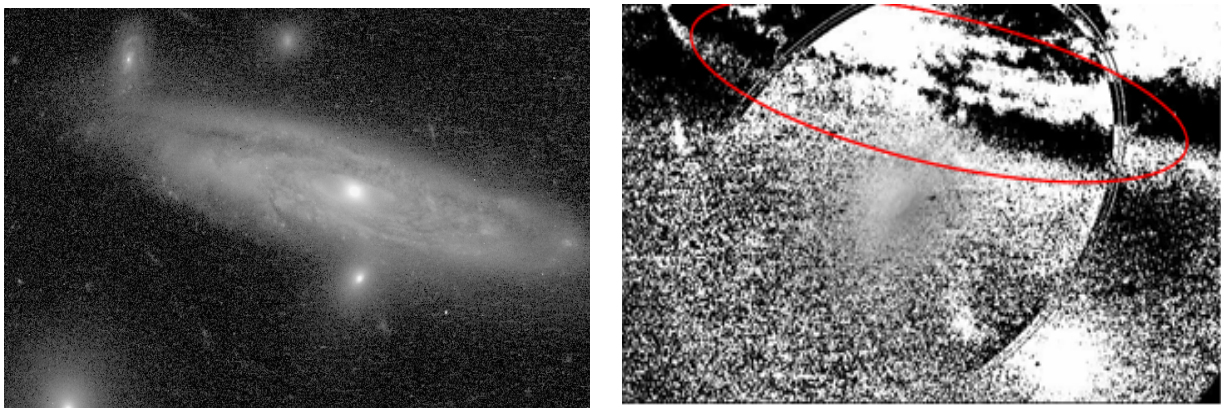

(a) Original SNAPshot Image of SDSS 0914

(b) Transmission Map with Annuli Indicating Limits of Foreground Galaxy

Figure 7.6: SDSS 0914: Edge of dust structure from the SNAPshot image and dust map

can be said about how much larger the galaxies appear as a result of backlighting, the edge of dust structure is evident in the SNAPshot images as well as the the transmission maps of both targets.

7.3 Transparency

One of the oldest questions when it comes to dust in spiral galaxies has dealt with the transparency of these systems. Initially thought to be completely opaque, (see Valentijn, 1990), the more common thought of late is that spiral galaxies appear to have regions of nearly opaque structure in addition to areas that may be completely transparent. We investigated these claims for all nine of the STARSMOG targets selected for this study, specifically in the regions of backlit dust. All nine targets appear to have a wide range of transparencies, even for such a small region as compared to the size of the foreground galaxies. Figure 7.8 indicates how each target displays a wide range of transmission percentages within the regions of backlit dust (where "0.0" on the transmission scale indicates a completely opaque area, and a transmission of "1.0" is completely transparent). Most systems have regions above 1.0 but as is it purely unphysical to have more than 100% transmission, these values give indications as to the errors in the transmission maps used to create this plot (and the individual transparency plots shown in Chapter 6). For example, SDSS 2205 may not have been the ideal candidate for this type of transmission

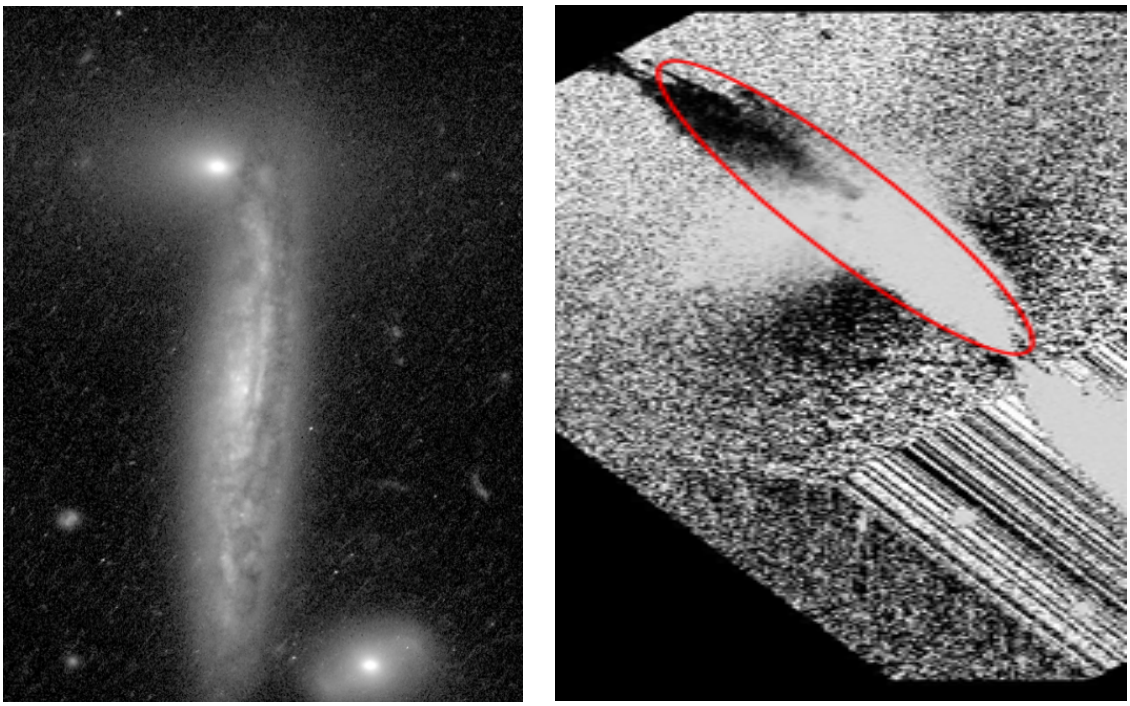

(a) Original SNAPshot Image of SDSS 2205

(b) Transmission Map with Annuli Indicating Limits of Foreground Galaxy

Figure 7.7: SDSS 2205: Edge of dust structure from the SNAPshot image and dust map

modeling given that based on the figure 7.8, 80% of the backlit region has transmission outside the physical regime.

To investigate the accuracy of the transmission maps on a pixel-by-pixel basis, we did simple error analysis calculations (using the standard deviation and average pixel value for regions of the image where the light could be attributed to either the foreground or background galaxy), the results of which are outlined in table 7.2. The errors from the individual contributions of the foreground and background galaxies were added in quadrature in order to produce a final error estimate for each target. These calculated errors are for the statistics of a single pixel, near the median properties of pixels in the overlap region. Averaging over multiple pixels will decrease the purely statistical error (although not necessarily systematic errors caused by, for example, actual asymmetry, especially in the foreground galaxy). As previously discussed, SDSS 2116 did not respond well to this type of analysis, a fact that is reflected in the high error estimate.

With regard to transparency, we also investigated how the presence of a bar effected the transmission results. To do so, we've focused on three opacities (10%, 50%, and 90%

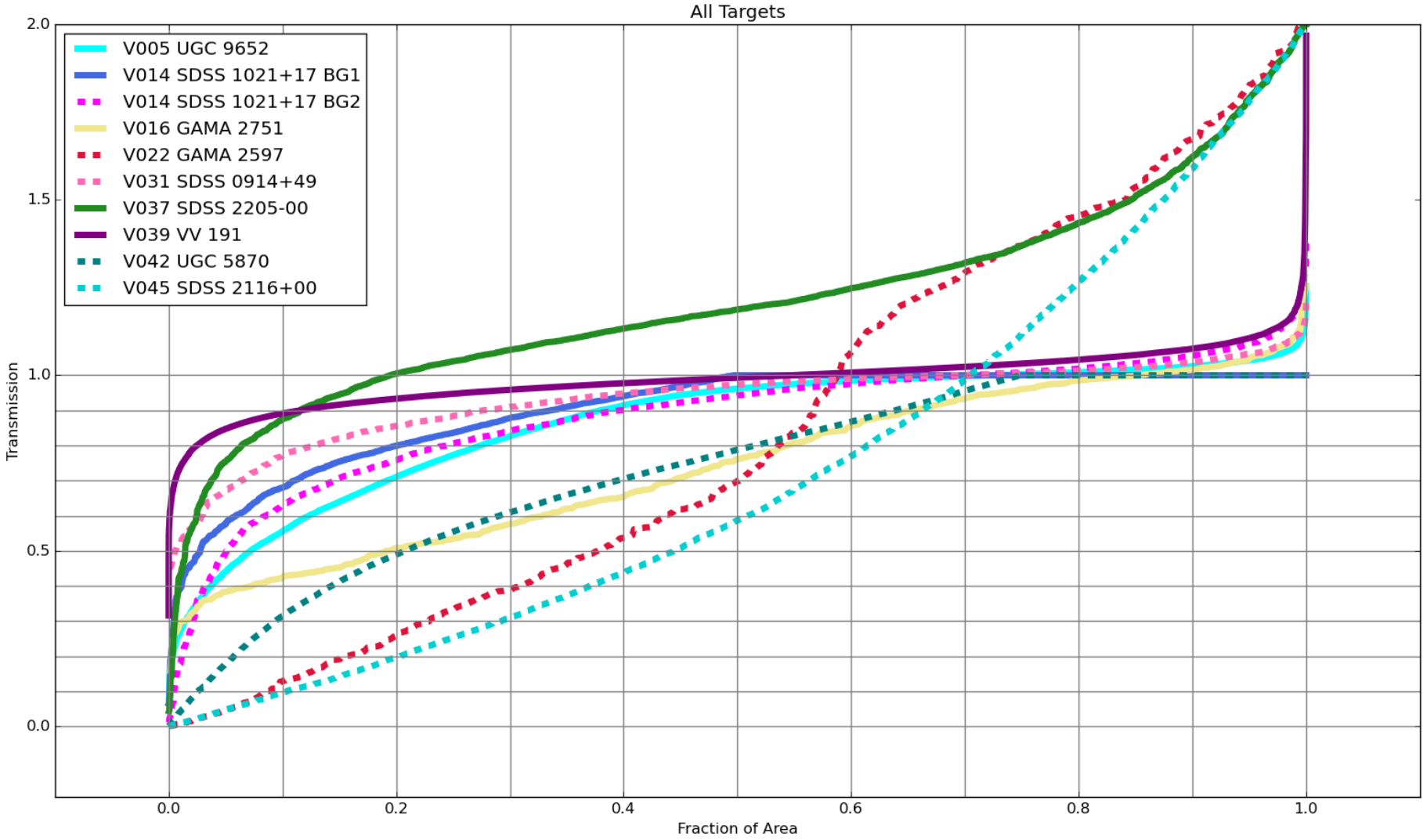

Figure 7.8: Transparency plot of All Targets

Table 7.2: Error Estimates of Transmission Maps

Object	BG Error Contribution	FG Error Contribution	Final Error Estimation
UGC 9652 region 1	0.012	0.075	0.076
UGC 9652 region 2	0.012	0.031	0.034
SDSS 1021 BG 1	0.030	0.040	0.050
SDSS 1021 BG 2	0.012	0.033	0.035
GAMA 2751	0.014	0.094	0.095
GAMA 2597	0.037	0.083	0.091
SDSS 0914	0.025	0.094	0.097
SDSS 2205	0.020	0.279	0.280
VV 191	0.035	0.003	0.035
UGC 5870	0.024	0.115	0.117
SDSS 2116	0.013	1.30	1.30

transmission) and plotted the average radius of backlit dust structure as a function of covering fraction at each of these transmission percentages. Based on these plots, shown in figures 7.9, 7.10, and 7.11 respectively, there does not appear to be a link between the presence of a bar and the covering fraction fraction at any given transmission percentage. We do notice that GAMA 2597 and SDSS 2116 (two highest data points in all three plots) have consistently high covering fraction despite having low to moderate transmission. UGC 9652, SDSS 1021, and SDSS 2205 on the other hand, have consistently low covering fraction for low to moderate transmission. Our next step would be to identify what each of these sets of targets had in common.

7.4 Statistics

In an attempt to identify the global galaxy properties which could give an indication as to the opacities of spiral systems in the future, we compared a variety of physical properties to the transmission percentages in order to identify any patterns that might arise. Figure 7.12 plots the average radius of the backlit dust against the transmission percentages and is organized by Hubble Type. Based on this plot, we are not led to believe there is any correlation in the data.

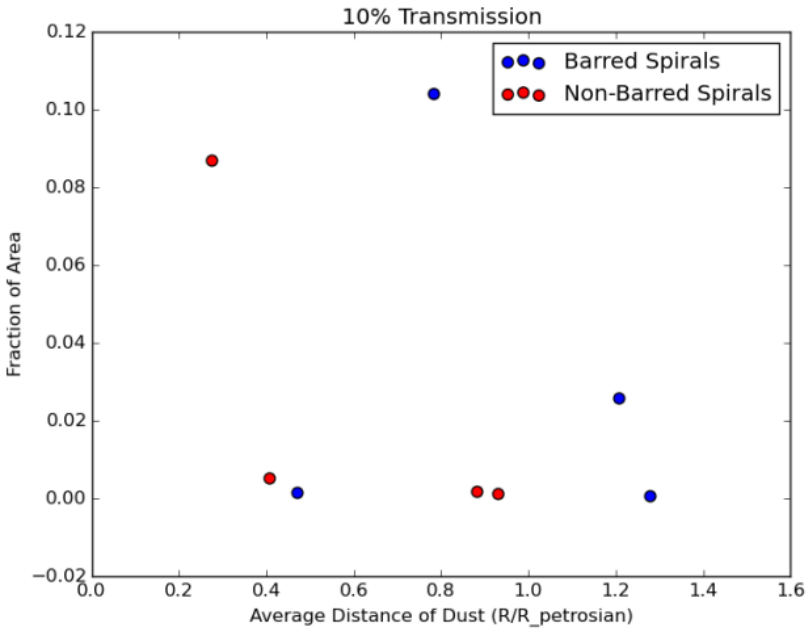

Figure 7.9: Radius of backlit dust as a function of covering fraction at 10% transmission

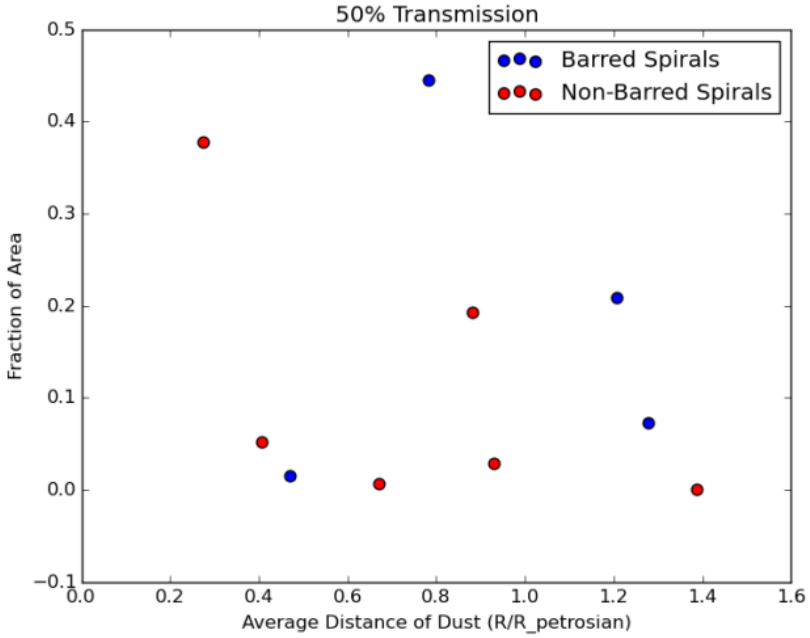

Figure 7.10: Radius of backlit dust as a function of covering fraction at 50% transmission

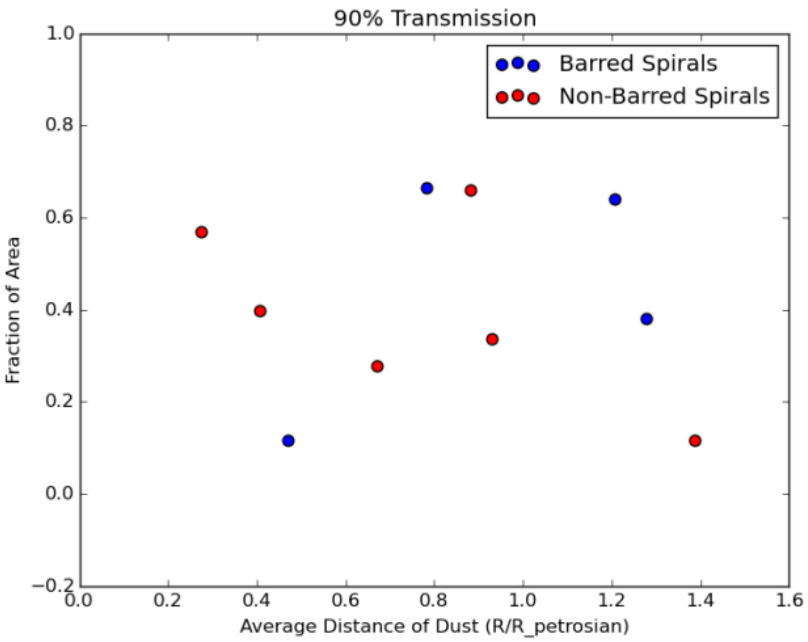

Figure 7.11: Radius of backlit dust as a function of covering fraction at 90% transmission

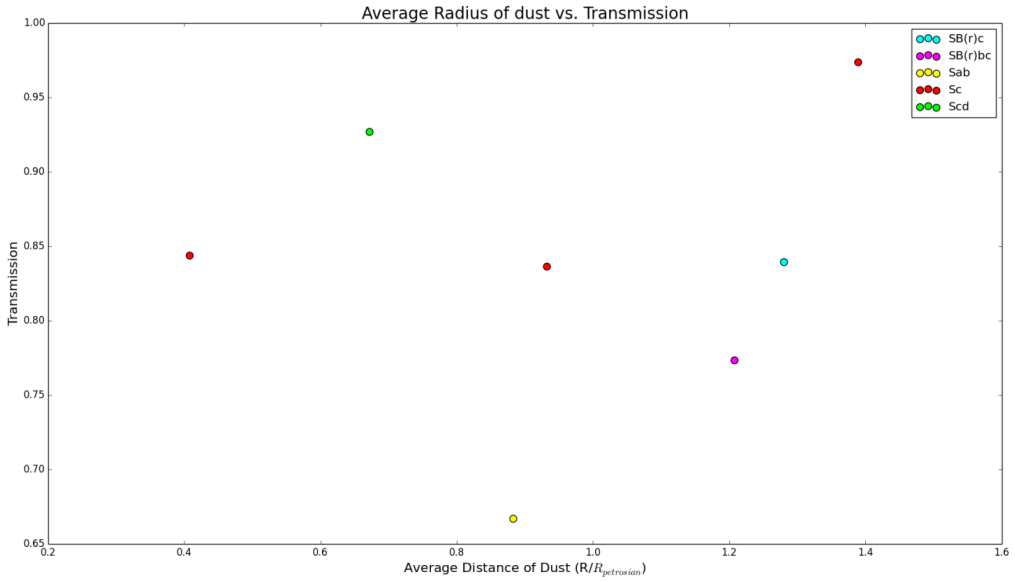

Figure 7.12: Average radius of backlit dust vs. transmission; Organized by Hubble type

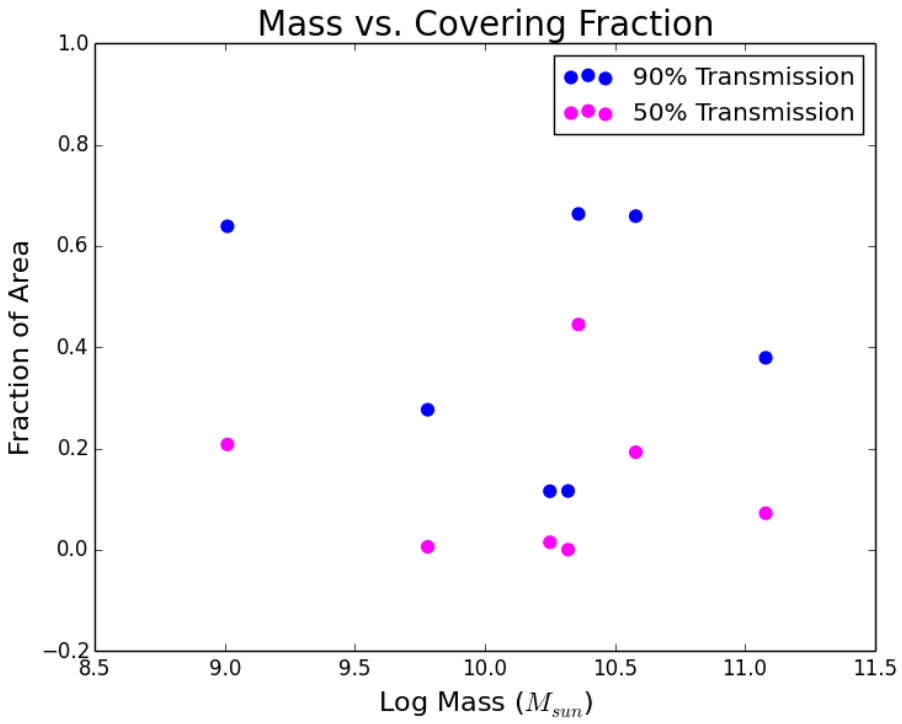

Figure 7.13: Log Mass versus Covering Fraction

Figures 7.13 and 7.14 compare the mass and star formation rates of the foreground galaxy, respectively, with the covering fraction at 50% and 90% transmission. From them, we see that relatively high mass targets have relatively low star formation rates which implies that the mass may be concentrated more in the bulge, rather than the spiral arms where star formation is more likely to occur. We also notice that moderately transparent systems have the highest star formation rates yet the lowest mass. Without quantitatively describing errors and given the limited number targets selected for this study, it is not clear if these correlations are statistically significant or if they are representative of the entire STARSMOG survey of occulting galaxy pairs.

Finally, we compared the average radius of the backlit dust with the average transmission percentage over the entire backlit region. When organized as either high or low mass ("low" mass was classified as Log Mass less than 10.25, and "high" mass as greater than 10.25) we see no distinct trend to the data (see fig 7.15). Both classifications have targets which span a wide range of both average dust radius and average transmission percentage. The more interesting comparison is a similar plot, Figure 7.16, which plots

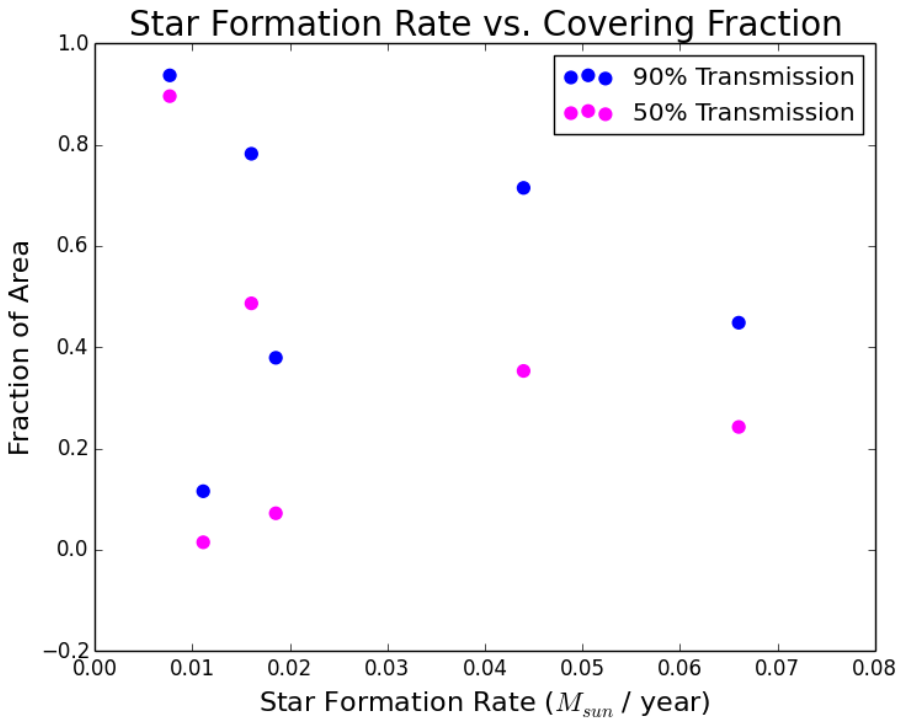

Figure 7.14: Star Formation Rate versus Covering Fraction

the average radius of the backlit dust and average transmission percentage for foreground galaxies but is organized by high and low star formation rates. "High" indicates foreground galaxies with star formation rates greater than 0.03 solar masses per year, and any systems with star formation rates lower than 0.03 solar masses per year are classified as "low". Despite having even fewer data points, targets with the least star formation appear dustier (more opaque) than those with higher star formation rates. This preliminary data lends itself to further investigation for the rest of the STARSMOG targets and other occulting galaxies on which this technique may be applied.

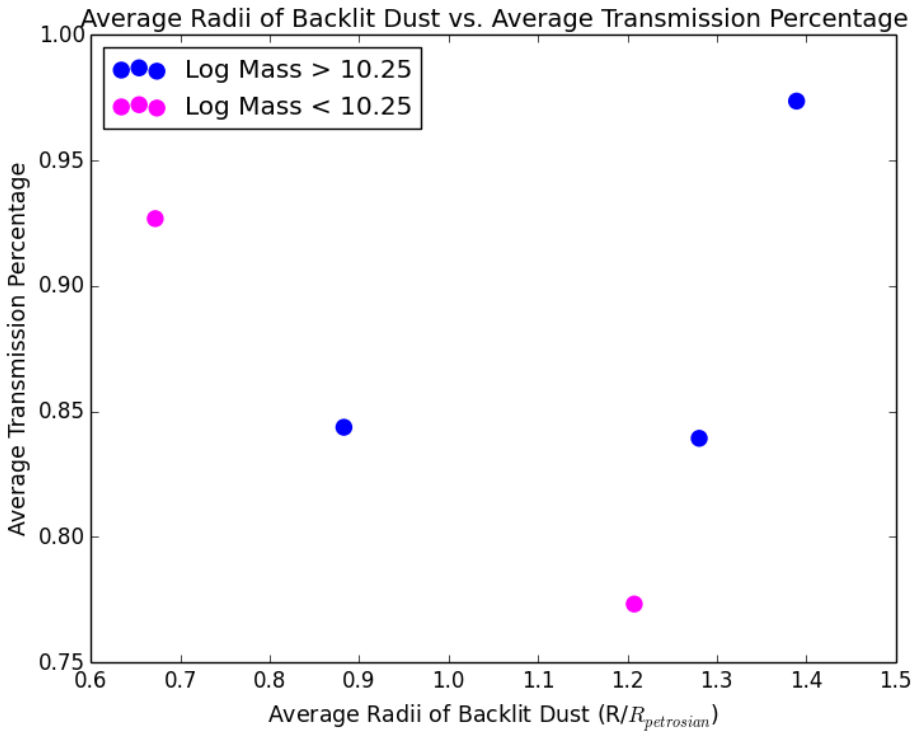

Figure 7.15: Radii of backlit dust vs. transmission percentage for high/low mass galaxies

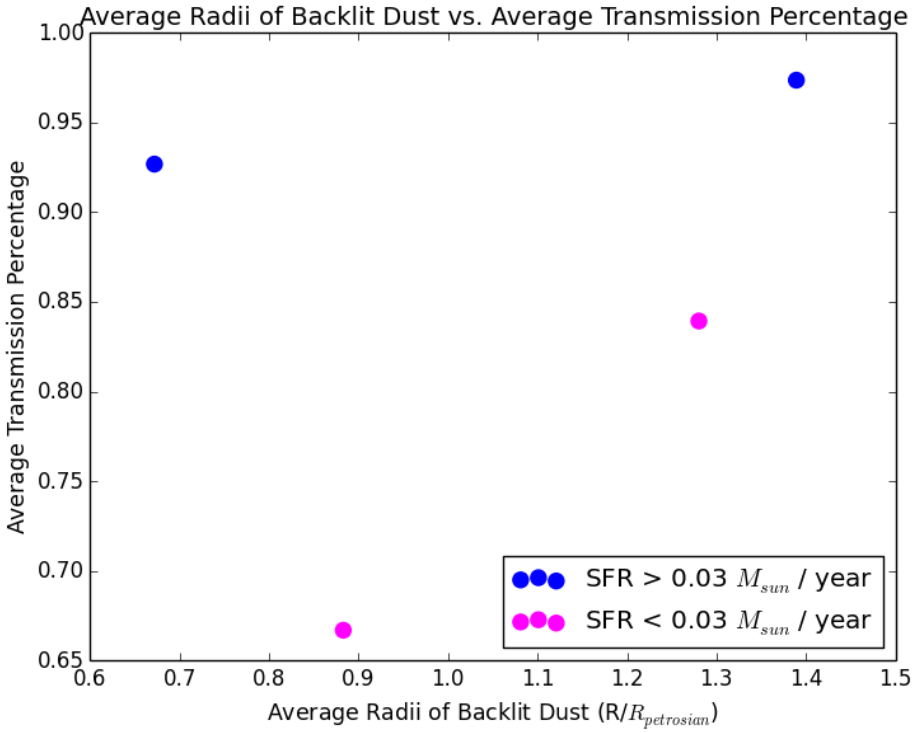

Figure 7.16: Radii of backlit dust vs. transmission percentage by star formation rates

CHAPTER 8

CONCLUSIONS

The dust in spiral galaxies has been known to play a big role in our observations because of its interaction with starlight, while it may not be considered one of the most "fundamental" problems in astronomy, the impact that dust in spiral disks has on these problems is certainly non-trivial (Disney, 1995).

We used the "Occulting-Galaxies" technique, based on White & Keel (1992), to investigate the properties of dust structure in nine targets mined from the STARSMOG catalog (see Holwerda, 2014). These nine targets were selected based on their symmetry and how closely each resembled the "ideal" target for using this technique. By exploiting symmetry in each system we first created transmission maps to observe the over- and under-densities in the dust structure among regions of backlit dust in the foreground galaxy.

The transmission maps themselves show over-densities in the dust structure (namely, dust lanes) which do not always follow the pitch angle of the spiral arms in late-type spirals. For some targets, these dust lanes criss-cross in a "web-like" pattern with little regard to the direction of the spiral arms. While this observation is hardly considered "new", the fact that we only see this type of pattern in late-type spirals (SBc/Sc/Sbc) is interesting enough to warrant addition study as new targets accumulate.

The opacity of spiral disks was one of the earliest problems associated with dust in spiral galaxies. The debate early-on (circa 1990) was whether spirals in general could be classified as either completely opaque or completely transparent. As is the case in most debates, the answer appeared to lie somewhere in the middle. Most subsequent studies have found that spiral disks have regions of both high and low opacity. By using the transmission maps from this study we were able to investigate the opacity within the

small region of backlit dust of the foreground spiral and found that our results are in agreement with this "middle-of-the-road" conclusion. Even in this small backlit region, we see the entire range of opacities (from completely transparent to completely opaque) for all nine of the targets, making it unfair to classify any one of them as either completely transparent or completely opaque.

One of the more surprising observations from the resultant transmission maps was the clearly-defined edge (or maximum radius) to the dust structure. While this observation depended mostly on the geometry of the system (inclination angle, how far out in radius the backlit dust was from the foreground nucleus, etc.) we were able to observe this edge for three of the targets with the most optimal orientation. The most interesting case seen of this edge was for target VV 191, where the location of the backlit dust actually included the maximum radius to the dust structure. In this case, the disk of the foreground galaxy appears nearly twice as large as might have been assumed without this background galaxy illuminating the dust structure further away from the foreground galaxy nucleus.

While there appears to be no real trend in the statistics of transmission through backlit dust with respect to stellar mass of the galaxies, there does appear to be a correlation with respect to star formation rates. In this nine-system sample, the targets with the least star formation appear the most opaque. By continuing this study for the rest of the STARSMOG targets, we will be able to determine how representative this sample is of the entire target set. While the currently limited sample size does not lend itself to make any definite conclusions based on the statistics of this study, it does give enough reason to investigate the statistics further once a larger sample of viable systems becomes available.

REFERENCES

Block, D. L., Witt, A. N., Grosbol, P., Stockton, A., & Moneti, A. 1994, AAP, 288, 383

Bosma, A., Byun, Y., Freeman, K. C., & Athanassoula, E. 1992, APJL, 400, L21

Burstein, D., Haynes, M. P., & Faber, M. 1991, NAT, 353, 515

Burstein, D., Willick, J., & Courteau, S. 1995, in NATO Advanced Science Institutes (ASI) Series C, Vol. 469, NATO Advanced Science Institutes (ASI) Series C, ed. J. I. Davies & D. Burstein, 73

Byun, Y.-I. 1993, PASP, 105, 993

Curtis, H. D. 1918, Publications of Lick Observatory, 13, 43

de Vaucouleurs, G., de Vaucouleurs, A., & Corwin, J. R. 1976, in Second reference catalogue of bright galaxies, 1976, Austin: University of Texas Press., 0

Disney, M. 1995, in NATO Advanced Science Institutes (ASI) Series C, Vol. 469, NATO Advanced Science Institutes (ASI) Series C, ed. J. I. Davies & D. Burstein, 5

Disney, M., Davies, J., & Phillipps, S. 1989, MNRAS, 239, 939

Domingue, D. L., Keel, W. C., & White, III, R. E. 2000, ApJ, 545, 171

Draine, B. T. 2003, ARAA, 41, 241

Driver, S. P., Popescu, C. C., Tuffs, R. J., et al. 2008, APJL, 678, L101

Elmegreen, D. M. 1980, ApJS, 43, 37

Goad, J. W., & Roberts, M. S. 1981, ApJ, 250, 79

González, R. A., Allen, R. J., Dirsch, B., et al. 1998, ApJ, 506, 152

Holmberg, E. 1958, Meddelanden fran Lunds Astronomiska Observatorium Serie II, 136, 1

Holwerda, B. 2014, STarlight Absorption Reduction through a Survey of Multiple Occulting Galaxies (STARSMOG), HST Proposal

Holwerda, B. W., Böker, T., Dalcanton, J. J., Keel, W. C., & de Jong, R. S. 2013, mnras, 433, 47

Holwerda, B. W., Keel, W. C., Williams, B., Dalcanton, J. J., & de Jong, R. S. 2009, aj, 137, 3000

Huizinga, J. E. 1994, PhD thesis, PhD thesis, Univ. Groningen, The Netherlands , (1994)

James, P. A., & Puxley, P. J. 1993, NAT, 363, 240

Jedrzejewski, R. I. 1987, MNRAS, 226, 747

Keel, W. C., Manning, A. M., Holwerda, B. W., et al. 2013, PASP, 125, 2

Keel, W. C., & White, III, R. E. 2001a, AJ, 121, 1442

—. 2001b, AJ, 122, 1369

Lauberts, A., & Valentijn, E. A. 1989, The surface photometry catalogue of the ESO-Uppsala galaxies

Misiriotis, A. 2005, AAP, 440, 67

Pogge, R. 2015, IV Interstellar Dust, `http://www.astronomy.ohio-state.edu/~pogge/Ast871/Notes/Dust.pdf`

Tody, D. 1986, in procspie, Vol. 627, Instrumentation in astronomy VI, ed. D. L. Crawford, 733

Tody, D. 1993, in Astronomical Society of the Pacific Conference Series, Vol. 52, Astronomical Data Analysis Software and Systems II, ed. R. J. Hanisch, R. J. V. Brissenden, & J. Barnes, 173

Valentijn, E. A. 1990, NAT, 346, 153

Viaene, S., Baes, M., Bendo, G., et al. 2015, ArXiv e-prints, arXiv:1511.07430

White, R. E., & Keel, W. C. 1992, NAT, 359, 655

White, III, R. E., Keel, W. C., & Conselice, C. J. 2000, ApJ, 542, 761

Witt, A. N., Thronson, Jr., H. A., & Capuano, Jr., J. M. 1992, ApJ, 393, 611